Atmos. Chem. Phys. Discuss., 12, 23333–23401, 2012
www.atmos-chem-phys-discuss.net/12/23333/2012/
doi:10.5194/acpd-12-23333-2012

Atmospheric Chemistry and Physics Discussions

Long term measurements of aerosol optical properties at a pristine forest site in Amazonia

L. V. Rizzo[1], P. Artaxo[2], T. Müller[3], A. Wiedensohler[3], M. Paixão[3], G. G. Cirino[4], A. Arana[2], E. Swietlicki[5], P. Roldin[5], E. O. Fors[5], K. T. Wiedemann[6], L. S. M. Leal[4], and M. Kulmala[7]

[1]Department of Earth and Exact Sciences, Institute of Environmental, Chemical and Pharmaceutics Sciences, Federal University of São Paulo, São Paulo, Brazil
[2]Department of Applied Physics, Institute of Physics, University of São Paulo, São Paulo, Brazil
[3]Leibniz Institute for Tropospheric Research, Leipzig, Germany
[4]National Institute for Amazonian Research (INPA), Manaus, Brazil
[5]Division of Nuclear Physics, Physics Institute, Lund University, Lund, Sweden
[6]Division of Engineering and Applied Science/Department of Earth and Planetary Science, Harvard University, Cambridge, USA
[7]Department of Physical Sciences, Division of Atmospheric Sciences, University of Helsinki, Helsinki, Finland

Received: 28 August 2012 – Accepted: 29 August 2012 – Published: 10 September 2012

Correspondence to: L. V. Rizzo (lrizzo@unifesp.br)

Published by Copernicus Publications on behalf of the European Geosciences Union.

ACPD

12, 23333–23401, 2012

Abstract

A long term experiment was conducted in a pristine area in the Amazon forest, with continuous in situ measurements of aerosol optical properties between February 2008 and April 2011, comprising, to our knowledge, the longest database ever in Amazonia. Two types of aerosol particles, with significantly different optical properties were identified: coarse mode predominant biogenic aerosols in the wet season (January–June), naturally released by the forest metabolism, and fine mode dominated biomass burning aerosols in the dry season (July–December), transported from regional fires. Dry particle median scattering coefficients at the wavelength of 550 nm increased from 6.3 Mm^{-1} to 22 Mm^{-1}, whereas absorption at 637 nm increased from 0.5 Mm^{-1} to 2.8 Mm^{-1} from wet to dry season. Most of the scattering in the dry season was attributed to the predominance of fine mode particles (40–80 % of PM_{10} mass), while the enhanced absorption coefficients are attributed to the presence of light absorbing aerosols from biomass burning. As both scattering and absorption increased in the dry season, the single scattering albedo (SSA) did not show a significant seasonal variability, in average 0.86 ± 0.08 at 637 nm for dry particles. Measured particle optical properties were used to estimate the aerosol forcing efficiency at the top of the atmosphere. Results indicate that in this pristine forest site the radiative balance was dominated by the cloud cover, or, in other words, the aerosol indirect effect predominated over the direct effect, particularly in the wet season. Due to the high cloud fractions, the aerosol forcing efficiency was below $-3.5\,W\,m^{-2}$ in 70 % of the wet season days and in 46 % of the dry season days. These values are lower than the ones reported in the literature, which are based on remote sensing data. Besides the seasonal variation, the influence of external aerosol sources was observed occasionally. Periods of influence of the Manaus urban plume were detected, characterized by a consistent increase on particle scattering (factor 2.5) and absorption coefficients (factor 5). Episodes of biomass burning and mineral dust particles advection from Africa were observed between January and April, characterized by enhanced concentrations of fine

ACPD

12, 23333–23401, 2012

mode ($PM_{2.0}$), crustal elements (Al, Si, Ti, Fe) and potassium. During these episodes, median particle absorption coefficients increased by a factor of 2, whereas median SSA values decreased by 7 %, in comparison to wet season conditions.

1 Introduction

The Amazon Basin constitutes a unique place for studying the impact of anthropogenic activities over natural atmospheric conditions. Under pristine circumstances, Amazonian aerosol particles come mostly from biogenic sources, with mass concentrations in the order of 10 $\mu g\,m^{-3}$ and number concentrations ranging between 300 and 500 cm^{-3} (Martin et al., 2010a). This concentration range is among the lowest found on any continental site, and is similar to observations over remote oceans (Andreae, 2009). For example, observations in a remote continental site in Pallas, Finland, found aerosol concentrations of 410 cm^{-3} in average (Komppula et al., 2005); observations taken over the Indian Ocean report 361 cm^{-3} in average (Hudson and Yum, 2002). Since the mid 20th century, the region has been going through changes due to the expansion of agriculture, logging and urban areas (Davidson et al., 2012). As a consequence of these changes, a large amount of aerosols and trace gases have been added to the natural biogenic emissions, with impacts on the radiative budget in regional and global scale (Koren et al., 2004; Procopio et al., 2004; Sena et al., 2012).

In the last 20 yr, Amazonian aerosol particles have been the subject of a number of intensive studies, aiming for its characterization at pristine forest sites (Martin et al., 2010b; Zhou et al., 2002; Artaxo and Hansson, 1995) and at disturbed areas (Kaufman et al., 1998; Artaxo et al., 2002; Andreae et al., 2004). In-situ long-term observations in Amazonia have been conducted only for aerosol particle mass and its elemental composition (Artaxo et al., 1994).

To fill the gap of continuous aerosol monitoring in Amazonia and its interactions with climate, a forest reserve north of Manaus, Brazil, was chosen as one of the four EUCAARI (European Integrated Project on Aerosol Cloud Climate and Air

ACPD
12, 23333–23401, 2012

Quality interactions, Kulmala et al., 2011) measurement sites in developing countries. Under the framework of the EUCAARI project, measurements of aerosol physical and chemical properties were conducted between 2008 and 2009. Afterwards, it became a permanent measurement station in Amazonia, being maintained since 2010 under the scope of the AEROCLIMA project (direct and indirect effects of aerosols on climate in Amazonia and Pantanal). The establishment of this permanent monitoring site provided, to our knowledge, the longest time series of in situ aerosol observations in Amazonia, using state of art equipment. This paper focus on aerosol optical properties observed between 2008 and 2011.

The relevance of optical properties resides in the fact that aerosol particles interact with solar radiation with impacts on the regional radiation budget, climate and cloud properties (Hansen et al., 1997; Fan et al., 2008; Shindell and Faluvegi 2009). The fourth IPCC assessment report (Forster et al., 2007) attributes a wide range of uncertainty to the aerosol forcing on climate, with implications to climate model projections related to uncertainties in model parameters (Haerter et al., 2009). Loeb and Su (2010) stated that the direct aerosol radiative forcing uncertainty due to perturbations on aerosol particles' physical parameters is 0.5–1.0 $W m^{-2}$, with most of the uncertainty associated with aerosol single scattering albedo (SSA). Therefore, it is important to characterize accurately the optical properties of representative types of ambient aerosol particles to assess its impact on the Earth's energy budget and climate change.

The aim of this paper is to present a systematic analysis of aerosol particle optical properties in a pristine forest site, its annual variability, seasonality and relationships with aerosol particle mass, number concentration and particle number size distribution. As will be discussed along the paper, in spite of the fact that the measurement site is located in a pristine forest area, it is influenced by external aerosol sources like regional biomass burning, urban plumes and African dust advection. The impact of these external sources over the optical properties of natural aerosol population will be investigated, as well as the consequences over the aerosol forcing efficiency.

ACPD
12, 23333–23401, 2012

2 Experimental

2.1 Measurement site

Measurement of aerosol particle properties were taken from February 2008 to May 2011 at the Cuieiras forest reservation in Central Amazonia (Fig. 1), located 60 km NNW of Manaus, a developing city with a population of 1.8 million people (IBGE, 2011). The site is relatively undisturbed, in the sense that no biomass burning occurs in the reservation. Most of the time, the prevailing trade winds blow over vast expanses of intact tropical forest before reaching the measurement tower (TT34) (2° 35.6570 S, 60° 12.5570 W, 110 m a.s.l.). However, as will be further discussed, the site was affected by regional transport of pollutants, either from biomass burning or urban plumes.

All measurements were taken under dry conditions (RH 30–40 %), assured by an automatic diffusion dryer (Tuch et al., 2009). An inlet with an aerodynamic cutoff nominally of PM_{10}, but actually of PM_7 for our flow conditions, was used for laminar-flow aerosol sampling. Inlet lines ran from the measurement level (39 m, about 10 m above the canopy height) to an air conditioned container at ground level. Housing for the researchers and a diesel generator that provided power supply were located, respectively 0.33 km and 0.72 km to the west of the sampling site (downwind). A detailed description of the measurement site and surrounding can be found in Martin et al. (2010b).

2.2 Instrumentation

Aerosol particle scattering coefficients were measured using a three wavelength integrating nephelometer (TSI Model 3563) operating at 450, 550 and 700 nm (Anderson et al., 1996). The instrument was regularly calibrated using filtered air and CO_2. Sampling time varied between 1 and 5 min. The backscatter shutter engine worked only a part of the time, between November 2009 and September 2010. Data was corrected for truncation errors according to Anderson and Ogren (1998), using the tabulated factors for total scatter as a linear function of Ångström exponent with no cutoff at the

ACPD
12, 23333–23401, 2012

inlet. The average correction factor for truncation errors was 1.13 ± 0.08 for scattering coefficients at 550 nm. As will be discussed on Sect. 4.5, this truncation correction factor fits well to Mie calculated correction factors. A constant correction factor of 0.982 was applied to backscatter measurements at 550 nm, also according to Anderson and Ogren (1998). Due to the low aerosol loadings observed in Amazonia, aerosol particle optical data was averaged over 30 min intervals to improve statistics. Considering this averaging time, the detection limit of the Nephelometer at 550 nm is 0.14 Mm^{-1} (Anderson et al., 1996). Uncertainties for nephelometer measurements as a function of averaging time and loading were calculated according to Sheridan et al. (2002) and references therein. Total uncertainty associated with scattering measurements was calculated for 30 min averaging times as the root-sum-square of five error sources: instrument noise (5 % for $\sigma_s(550) = 1\,Mm^{-1}$ and 0.13 % for $\sigma_s(550) = 100\,Mm^{-1}$); drift ($\sim 3$ %); uncertainty in calibration (7 %); uncertainty associated to the truncation error correction (2.2 % for sub micrometer and 28 % for super micrometer aerosols); uncertainty of adjusting scattering coefficients to standard temperature and pressure (0.42 %). Similar calculations were performed to estimate the uncertainty of back scattering measurements. Tables 1 and 2 show the total uncertainties on scattering ($\delta\sigma_s$) and backscattering measurements ($\delta\sigma_{bs}$).

Aerosol particle absorption was measured using a MAAP photometer (MultiAngle Absorption Photometry – Thermo Inc., Model 5012) (Petzold et al., 2005), operating in series with the Nephelometer. The MAAP reports black carbon (BC) concentrations at 637 nm, which were converted to absorption coefficients assuming a mass absorption coefficient of 6.6 $m^2\,g^{-1}$, used in the firmware of the instrument. Particle absorption coefficients were measured every minute, and a 5 % correction was applied to the data to account for an adjustment of wavelength (Müller et al., 2011). 30 min averages were taken to improve statistics, with a resulting detection limit of 0.13 Mm^{-1} (Petzold et al., 2005). Pressure and temperature measured inside the Nephelometer were used for adjusting scattering and absorption coefficients to 1013.25 mbar and 0 °C. Between September and December 2008, integrating nephelometer measurements were

ACPD
12, 23333–23401, 2012

discontinued due to the need of maintenance, and the MAAP ran by itself under the diffusion dryer inlet. In this case, the temperature of the aerosol sample measured at the diffusion dryer outlet and ambient pressure were used for standard temperature and pressure corrections. A recent intercomparison of absorption photometers report MAAP noise levels up to 0.22 Mm^{-1} for 1 min averaging time, unit to unit variability of 3 % and 0.62 % of the scattering seen as apparent absorption (Müller et al., 2011). Assuming that the instrument noise decreases with the square root of averaging time, total uncertainties on aerosol absorption measurements averaged each 30 min would be of 4 %.

In this work, scattering and backscattering coefficients will be preferably reported at 550 nm, to ease the association with satellite based aerosol measurements like MODIS. Absorption and other aerosol properties that rely on absorption coefficients will be preferably presented at 637 nm, to avoid additional errors related to the unknown absorption spectral dependency. In these cases, scattering coefficients will be interpolated to 637 nm using power law fits (c.f. Eq. 2).

Measurements of aerosol particle number size distribution, number concentration, mass and elemental composition were also taken, adding to the analysis and discussion of aerosol optical properties. Two fine mode mobility particle size spectrometers (10–500 nm) were interchangeably used: a TSI 3936 SMPS (Scanning Mobility Particle Sizer) and a custom-made SMPS designed at Lund University according to EUSAAR (European Supersites for Atmospheric Aerosol Research) standards (Wiedensohler et al., 2012). Coarse mode particle number size distributions were measured using an OPC-Grimm Model 1.109 (300 nm–20 µm) (Optical Particle Counter), whenever the instrument was available. Operating after the inlet, the actual cutoff of the OPC is at the optical diameter of 6 µm, assuming the aerosol density of 1.38 $g\,cm^{-3}$ (Rissler et al., 2006). Particle number concentrations were interchangeably measured with condensation particle counters (TSI CPC models 3010, 3785, 3772). Stacked Filter Units (SFU) were used to collect fine mode ($D_p < 2.0\,\mu m$) and coarse mode ($D_p > 2.0\,\mu m$) aerosols, with integrating periods ranging from 2 to 5 days. Nuclepore filters were analyzed for

ACPD
12, 23333–23401, 2012

particulate mass, following the measurement protocol of the US Environmental Protection Agency for weighing filters, and elemental composition, using particle-induced X-ray emission and X-ray fluorescence analysis.

2.3 Meteorological parameters

Meteorological parameters were measured at the K34 tower (2° 36.5450 S, 60° 12.5580 W, 130 m a.s.l.), located 1.6 km to the south of the aerosol sampling site, and maintained by the National Institute for Research in the Amazon (INPA). Meteorological and radiation parameters were logged on a Campbell CR-10 data logger with a sampling interval of 30 s and stored as 10 to 30 min averages.

Along the aerosol measurement period, daytime quartiles of temperature, RH and wind velocity were, respectively 24.5 to 29.5 °C, 65 to 90 %, and 1.38 to 2.78 $m\,s^{-1}$. The corresponding nocturnal quartiles were, respectively, 23.1 to 25.6 °C, 82 to 95 %, and 1.24 to 2.31 $m\,s^{-1}$. The quartiles of pressure were 993.5 to 996.7 mbar. A detailed description of climatological conditions can be found in Araújo et al. (2002). Here, only the meteorological parameters relevant for the interpretation of aerosol measurements will be discussed.

Figure 2 shows the monthly accumulated precipitation between January 2008 and June 2011. Based on this figure, wet season is hereby defined as the period between January and June, and dry season between July and December. This definition may not be strictly correct from the climatological point of view, but for the purpose of the current aerosol dataset interpretation this is a reasonable choice. Figure 3a shows the wind rose between January 2008 and June 2011. Easterly trade winds dominate at low levels, blowing over larger areas of undisturbed rain forest during the wet season. Nevertheless, during the dry season, biomass burning emissions from the Pará State (~ 1200 km from the sampling site) are transported through easterlies. In 13 % of time, wind blew from the direction where the diesel generator was located (240°–330°). Episodes of diesel generator emissions influencing the aerosol measurements were carefully inspected and removed from the data set, as will be further discussed

ACPD
12, 23333–23401, 2012

on Sect. 3.3. Figure 3b shows the wind rose for the months of June and July between 2008 and 2011. The wind was southeastern 20 % of the time, making the sampling site particularly susceptible to the urban plume of Manaus during these months.

3 Methods

3.1 Calculation of aerosol optical properties

The first optical property that can be derived from scattering and absorption measurements is the aerosol particle extinction coefficient (σ_e):

$$\sigma_e(\lambda) = \sigma_s(\lambda) + \sigma_a(\lambda), \quad (1)$$

where $\sigma_s(\lambda)$ and $\sigma_a(\lambda)$ are, respectively the particle scattering and absorption coefficients measured at wavelength λ. In this work, particle extinction coefficients will be reported at 637 nm, applying a power law interpolation over scattering coefficients to the wavelength in which absorption coefficients (σ_a) were measured.

Aerosol particle intensive properties are those that do not depend on the particle amount, and are related to intrinsic properties of the aerosols. In this study, four aerosol particle intensive properties will be investigated: the Ångström exponent for scattering ($å$), the hemispheric backscatter ratio (b), the single scattering albedo (ω_0) and the aerosol forcing efficiency ($\Delta F/AOD$).

The particle scattering coefficient decreases monotonically with wavelength. In the literature it is usual to approximate this wavelength dependency by a power-law expression (Ångström, 1929):

$$\sigma_s(\lambda) = B \cdot \lambda^{-å}, \quad (2)$$

where $å$ is known as the scattering Ångström exponent and B is a constant known as the turbidity coefficient. Power laws were fitted to each 30 min averaged spectrum, and

ACPD
12, 23333–23401, 2012

the exponent was taken as the Ångström exponent. Ångström exponents are indicative of the average size of the particle population. For monomodal particle number size distributions, Ångström exponents greater than 2 indicate the predominance of particles around 0.1 µm associated with urban pollution and biomass burning, and values smaller than 1 indicate large particles typically associated with sea salt and mineral dust (Schuster et al., 2006).

The hemispheric backscatter ratio (b) is defined as:

$$b(\lambda) = \frac{\sigma_{bs}(\lambda)}{\sigma_s(\lambda)}, \quad (3)$$

where σ_{bs} is the particle backscatter coefficient, i.e. the volume scattering function integrated between 90° and 180°, while the total scattering coefficient (σ_s) is integrated between 0° and 180°. The backscatter ratio provides an indication of the angular distribution of the light scattered by aerosol particles, a key property to determine the aerosol direct radiative forcing (Andrews et al., 2006). Some studies report an inverse relationship between b and particle size (e.g. Collaud Coen et al., 2007). Other studies argue that changes in the backscattering ratio can also be driven by particle shape, especially for data taken under dry conditions, when particle sphericity is not certain (Doherty et al., 2005).

The single scattering albedo (SSA) is a measure of the aerosol particle scattering strength relative to extinction. The scattering coefficients at the integrating nephelometer wavelengths (450, 550, 700 nm) were interpolated logarithmically to the wavelength in which absorption coefficients (σ_a) were measured to obtain the single-scattering albedo (ω_0) at 637 nm:

$$\omega_0 = \frac{\sigma_s}{\sigma_s + \sigma_a}. \quad (4)$$

For purely scattering aerosol particles (e.g. ammonium sulfate) ω_0 approaches 1.0. Mineral dust, biomass burning and urban aerosols typically show SSA values in the

ACPD
12, 23333–23401, 2012

range 0.92–0.94, 0.88–0.95 and 0.90–0.98, respectively, under ambient conditions (Dubovik et al., 2002).

The particle SSA and the backscatter ratio can be used to calculate the top of the atmosphere aerosol forcing (ΔF) per unit aerosol optical depth (AOD), also called aerosol forcing efficiency (e.g. Kaufman et al., 2005):

$$\frac{\Delta F}{\mathrm{AOD}} = -LS_0T_{\mathrm{at}}^2(1-A_{\mathrm{c}})\varpi\beta\left\{(1-R_{\mathrm{s}})^2-\left(\frac{2R_{\mathrm{s}}}{\beta}\right)\left[\frac{1}{\varpi}-1\right]\right\}, \quad (5)$$

where L is the day length (set to 0.5 in the tropics); $S_0 = 1370\,\mathrm{W\,m^{-2}}$ is the solar constant; T_{at} is the atmospheric transmissivity (set to 0.76); A_{c} is the fractional cloud amount; R_{s} is the surface reflectance; ϖ and β are the spectrally weighted particle SSA and backscatter fraction, respectively (Haywood and Shine, 1995). Here, the aerosol layer is assumed to be optically thin, β is independent of the zenith angle, and T_{at} is assumed to follow Beer's Law. The surface reflectance at the tower site was based on IGBP (International Geosphere Biosphere Programme) broadband albedo from CERES (Clouds and the Earth's Radiant Energy System), $R_{\mathrm{s}} = 0.13$ (300–5000 nm). The daily time series of cloud fraction at the tower site was taken from MODIS measurements on Terra and Aqua satellites (global $1^\circ \times 1^\circ$ daily level-3 cloud fraction, day only). $\sigma_{\mathrm{s}}(\lambda)$ and $b(\lambda)$ were calculated trough extrapolation of the spectral dependence in the range 450–700 nm to the broadband range (300–5000 nm). $\sigma_{\mathrm{a}}(\lambda)$ was calculated assuming a power law dependency on λ, with an absorption Ångström exponent of 1.3 (Rizzo et al., 2011). Spectrally weighted ϖ and β were calculated based on global spectral irradiance $D(\lambda)$ for a sun-facing 37° tilted surface and air mass coefficient of 1.5 (Hulstrom et al., 1985):

$$\beta = \frac{\int b(\lambda)D(\lambda)\mathrm{d}\lambda}{\int D(\lambda)\mathrm{d}\lambda} \quad \text{and} \quad \varpi = \frac{\int \varpi_0 D(\lambda)\mathrm{d}\lambda}{\int D(\lambda)\mathrm{d}\lambda}. \quad (6)$$

It is important to emphasize that the results presented here refer to dry aerosols (RH < 40 %). Aerosol particle optical properties may change significantly under

ACPD
12, 23333–23401, 2012

ambient humidity conditions. Rissler et al. (2006) and Zhou et al. (2002) state that Amazonian aerosols are only moderately hygroscopic, with growth factors ranging between 1.0–1.3 for 100 nm particles at 90 % RH. The impact of hygroscopic growth on the particle scattering coefficients in Amazonia has been investigated by (Kotchenruther and Hobbs, 1998), reporting an average increase of 16 % on scattering and a decrease of 10 to 20 % on backscatter ratio when RH rises from 30 to 80 %. The dependence of particle absorption coefficients as a function of RH is not currently known. On one hand, the water uptake by aerosol increases the particle diameter, enhancing the focusing effect (Bohren and Huffman, 1998), causing an increase of particle absorption coefficients. On the other hand, the refractive index of water is smaller than that of the non-absorbing particle components, which may cause a decrease on particle absorption coefficients depending on particle size (Nessler et al., 2005). Modeling studies for a highly polluted area in China report absorption humidification factors ranging between 0.9 and 1.2 at 80 % RH (Cheng et al., 2008). The impact of RH on scattering and absorption reflect on the particle SSA and forcing efficiency. Anderson et al. (1999) reports increase of 2–5 % on particle SSA and a decrease of 10–15 % on aerosol forcing efficiency along the shift from low to high RH conditions.

3.2 Optical closure study

An optical closure study was done for aerosol particle properties measured between 1 July–14 August 2009, period at which particle number size distribution measurements of the fine and coarse aerosol were available. A Mie code based on Bohren and Huffman (1998) was used to calculate the optical particle properties for the entire aerosol population, assuming homogeneous spherical particles. Using particle number size distribution, refractive index and wavelength of incident light as inputs, the code calculates aerosol particle scattering, backscattering and absorption coefficients, and also simulates the measured particle scattering signal considering the 7 to 170° integrating angle range of the TSI 3563 nephelometer and its non lambertian illumination function (Anderson et al., 1996).

ACPD
12, 23333–23401, 2012

Sub micrometer particle aerosol number size distributions were measured using a custom-made SMPS (10–500 nm). For the accumulation and part of the coarse mode, an OPC-Grimm (300 nm–6 µm under operation conditions) was used. Optical particle size spectrometers measure optical particle diameters, based on the assumption that the scattered light intensity is a monotonic function of particle size (Hinds, 1999). The calibration of these instruments is typically performed with monodisperse polystyrene latex particles, which have a refractive index of 1.59. The refractive index of ambient aerosols is usually lower than that, resulting in underestimation of particles sizes (Heim et al., 2000). Particularly, the OPC-Grimm measures scattering at 655 nm, with collecting angles between 29.5 and 150.5°. Response correction functions for the measured optical particle number size distributions were calculated using the same Mie code assuming a range of refractive indexes, and a look-up table was produced. The correction affects the bin boundaries of the OCP-derived optical diameter, resulting in a shift of geometric mean diameters and adjustment of normalized number concentrations, according to bin width change. Calculations have shown that 1 µm particles can be up to 30 % underestimated, depending on its refractive index. The correction factors increase with the imaginary part of the refractive index, particularly for super micrometer particles.

Particle number size distributions of the mobility and optical particle size spectrometers were 60 min averaged, and used as input to the Mie code. A range of refractive indexes (1.34 to 1.80 and 0 to 0.03 i, with steps of 0.005 and 0.0005, respectively) was tested for each combined particle number size distribution, with the corresponding OPC response adjustment taken from the mentioned look up table of correction factors. Corrected particle number size distributions were truncated at the optical diameter of 6 µm. The refractive index representative of each size distribution was iteratively determined by means of matching calculated and measured scattering and absorption coefficients within 10 %. This confidence range is similar to the usual expected data quality of particle size spectrometers (Wiedensohler et al., 2012).

ACPD
12, 23333–23401, 2012

3.3 Classification of aerosol external sources

In spite of the fact that the measurement tower is located in an area of undisturbed primary forest, it sporadically received the influence of external aerosol sources: (1) local pollution (diesel generator and occasional vehicles transporting researchers and equipment); (2) Manaus urban plume; (3) regional transport of biomass burning emissions; (4) soil dust and biomass burning transport from Northern and Equatorial Africa. The local pollution source and the Manaus urban plume were most significant during the wet season, occasionally affecting pristine conditions of low aerosol particle mass concentration. Figure 4 shows median aerosol particle number concentration as a function of wind direction, in which the signal of the Manaus urban plume and of the diesel generator is clear during the wet season. The same figure shows that during the dry season the transport of regional biomass burning emissions overcame all other external sources.

Local pollution episodes were characterized by abrupt changes in particles number concentrations, typically lasting from 30 to 3 h. Periods of western and northwestern wind direction (270 to 340°), where the diesel generator was located, were scrutinized, and the aerosol particle data associated with local pollution was excluded from the analysis, comprising 2 % of the measurement period.

The Manaus urban plume reached the sampling site sporadically, with effects lasting from 4 h to a whole day. The greater time extent of the Manaus plume compared to that of the generator is due to their respective horizontal scales. Episodes were characterized by a consistent increase on aerosol particle number concentrations, scattering and absorption coefficients, as will be further discussed on Sect. 4.6.1. Periods with local wind directions coming from Manaus city (120–190°) were carefully inspected, and HYSPLIT back-trajectories (Draxler and Rolph, 2012; Rolph, 2012) were calculated to verify the origin or air masses reaching the site. Back-trajectories were based on meteorological REANALYSIS dataset, with 24 h total run time, starting at 50 m height.

ACPD
12, 23333–23401, 2012

Confirmed Manaus urban plume transport events comprised 1.5 % of the measurement period, and were not removed from the data analysis.

Transport of biomass burning emissions from Eastern Amazonia occurred all through the dry season period, being the strongest non-biogenic aerosol source reaching the measurement site. In the dry season, pollution from biomass smoke typically accounts for > 90 % of the fine particles and ∼ 50 % of the coarse particle mass (Martin et al., 2010). Table 3 shows the fire spots detected for the dry seasons of 2008, 2009 and 2010 (July–December) in Amazonia by the polar satellites NOAA 15–19 and AQUA, and by the geostationary satellite GOES-12, operationally processed by the Brazilian National Institute of Spatial Research (CPTEC/INPE). A spot indicates the occurrence of fire in one pixel, i.e. 1–20 km^2 depending on the satellite resolution. The fire counts shown here are overestimated, since the same burning event can occasionally be detected by two satellites in different positions (a couple of km difference), in a way that a single fire spot may be counted twice. Fire counts in the Amazonas State, where the ZF2 forest reserve is located, are 90 % smaller than the fire counts in its eastern neighbor Pará State. Fire counts in the legal Amazonia area significantly increased in 2010, probably due to the severe drought that occurred in that year (Lewis et al., 2011). In 2009, fire spots at districts neighbor and eastern to the ZF2 forest reserve showed a noteworthy increase, echoing on aerosol optical properties, as will be further discussed.

There is evidence that the research site was affected at times by soil dust transport from Northern Africa and biomass burning from Equatorial Africa. This is supported by satellite observations (Kaufman et al., 2005), LIDAR measurements (Ansmann et al., 2009; Baars et al., 2011); back-trajectories analysis and surface measurements (Ben-Ami et al., 2010; Prenni et al., 2009). At the research site, African mineral dust advection can be traced by increased concentrations of crustal elements Al, Si, Ti and Fe on fine mode aerosol filter samples. African mineral dust transport events are typical to the months of March and April, while advection of African biomass burning aerosols occurs also in the dry season (Martin et al., 2010a). The periods of

ACPD
12, 23333–23401, 2012

influence of African aerosols advection in the wet season of 2008 are well documented by Baars et al. (2011), and will be used in this study to calculate statistics for aerosol properties under this condition (Table 4). According to the same study, the episodes of African aerosol advection that occurred in the wet season of 2008 showed dust fractions ranging from 20 to 100 %. The non-dust fraction was mostly related to aged biomass burning aerosols from Africa. Based on the spectral dependency of LIDAR ratios, the authors state that the influence of marine aerosol particles and local pollution was not significant during those events.

4 Results and discussion

4.1 Variability of aerosol optical properties

The complete time series of aerosol particle scattering and absorption coefficients is illustrated in Figs. 5 and 6. Year to year variability on aerosol particle optical properties occurred mostly due to deviations on the amount of precipitation and biomass burning sources strength. Table 5 shows that the 2009 dry season had median values of aerosol particle scattering and absorption, respectively 110 % and 23 % greater than the values observed during the dry season of 2010. This is an outcome of the increased occurrence of fire spots at neighbor municipalities and at districts located to the east of the forest reserve during the dry season of 2009 in comparison with 2008 and 2010 (Table 3). Particle scattering coefficients increased substantially under the influence of biomass burning particles. This is a consequence of enhanced concentration of fine mode particles in the dry season, which are more efficient to scatter light in comparison to the coarse mode dominated biogenic particles in the wet season.

Another feature shown in Table 5 is that the median value of the particle absorption in the wet season of 2010 was approximately 2.6 times greater than the values observed during the other years of measurements. Monthly median particle absorption coefficients were 4 times greater in January and February 2010 in comparison to

ACPD
12, 23333–23401, 2012

the same months in 2009 and 2011 (Fig. 7). No influence of the Manaus urban plume or fire spots in nearby districts was detected in this period. In January and February 2010, eight periods of elevated absorption coefficients ($> 2\,Mm^{-1}$) were observed, lasting continuously from 2 to 6 days. This time scale is typical of African aerosol advection events, and this is the most feasible explanation for the observed increase of absorption coefficients in the wet season of 2010. This hypothesis is supported by the monthly averages of fine mode crustal elements (Al, Si, Ti, Fe) and potassium (Fig. 8). Potassium in the fine mode has been associated both to biomass burning and to biogenic sources in the Amazon (Artaxo et al., 1994). Increased mass fractions of these elements between January and March 2010 suggest the advection of mineral dust and biomass burning aerosols from Africa.

Figure 9 puts together the time series of in-situ aerosol particle extinction, calculated from scattering and absorption coefficients measured above the canopy, and the time series of aerosol optical depth (AOD) from MODIS (TERRA-AQUA) and from AERONET sun photometer in Manaus. It is clear that the aerosol particle extinction measured right above the canopy echoes in the remotely sensed AOD in the entire atmospheric column. It is worth noticing that between January and April, when African advection events typically occur, the remotely sensed AOD often increased without a corresponding enhancement on in situ aerosol extinction. That can be explained by the fact that not all African advection events reach the surface, depending on atmospheric conditions.

In spite of the year to year variability, the dataset shows a clear seasonal pattern, with higher aerosol particle concentrations during the dry season (July–December) in comparison to the wet season (January–June). From wet to dry season, median aerosol particle scattering (550 nm) and absorption (637 nm) coefficients increased from 6.3 to $22\,Mm^{-1}$, and from 0.5 to $2.8\,Mm^{-1}$, respectively (Table 6). Figures 10 and 11 show box plots for particle scattering and absorption coefficients, calculated for each 10 Julian days between February 2008 and May 2011. Besides the seasonal variation related to dry and wet seasons, there is a clear influence of mineral dust and aged biomass

ACPD
12, 23333–23401, 2012

burning aerosol advection from Africa over the particle absorption coefficients between January and March, while the particle scattering coefficients were not significantly affected. This leads to decreased SSA, reaching values as low as 0.55 in March (Fig. 12). That explains, in part, the reason why the median SSA value is 0.88 both for wet and dry season (Table 6). This median value is in accordance with LIDAR derived SSA values in the main aerosol layer below 2.5 km height at the same forest reserve (Baars et al., 2012). The particle SSA measured in situ is also consistent with AERONET observations in the atmospheric column, considering that under ambient RH conditions the in situ dry aerosol particle SSA values would increase by 2–5 % (Anderson et al., 1999). Figure 13 shows monthly statistics for AERONET aerosol particle SSA between 1993 and 2011 at 7 different locations in Amazonia: 3 of them situated at the region of the so-called arc of deforestation (Ji Paraná, Alta Floresta and Rio Branco), and 4 of them at Northern Amazonia, far from direct impact of forest fires (Balbina, Belterra, Santarém and Manaus). There are few observations in the wet season because the inversion algorithm for particle SSA retrieval requires a minimum aerosol optical thickness of 0.4 (Holben et al., 2006), which is much greater than the average value of 0.15 observed in the wet season (Schafer et al., 2008). Also, in the wet season the steady cloud cover in Amazonia prevents the measurements of sky radiances. For the same reasons, AERONET SSA data is scarce at pristine forest sites (Northern Amazonia). Considering 129 data points in Northern Amazonia, the average AERONET SSA at 637 nm is 0.91 ± 0.03, whereas in the arc of deforestation 1815 data points result in an average value of 0.92 ± 0.03. Within the uncertainties, there is no particle SSA variability for regions in the arc of deforestation compared to relatively pristine regions.

Contrary to particle scattering and absorption coefficients, the Ångström exponent and the backscatter ratio did not show a clear seasonal pattern. Both parameters showed greater dispersion in the wet season, when the aerosol particle concentration was low and the instruments were operating close to its detection limit. The average Ångström exponent was 15 % greater in the dry season (Table 6), which could be an echo of increased concentration of fine mode biomass burning particles from

ACPD
12, 23333–23401, 2012

regional fires. The backscatter ratio at 550 nm had a median value of 0.15, without significant differences between the wet and dry seasons (Table 6). The relationship of the Ångström exponent and the backscatter ratio with particle size will be further discussed on Sect. 4.3.

Particle scattering and absorption coefficients showed an enhancement of approximately 50 % between 09:00 and 12:00 LT in the wet season (Fig. 14). In the wet season, sub micrometer aerosol particle number size distribution measurements showed an increase of 20 % in the count mean diameter at the same period of the day, while the integrated particle number concentrations kept rather constant. The daytime shift of sub micrometer particle diameters has also been observed in another site in Amazonia (Rissler et al., 2006), and may be attributed to the photochemical formation of secondary organic aerosols in the residual layer, mixing down to the ground as the boundary layer height increases in the morning hours. A Mie modeling exercise indicated that a 20 % increase on sub micrometer particle diameters may cause an increase of 50–70 % on scattering coefficients and 10–40 % on absorption coefficients. In the dry season, the regional transport of biomass burning particles seems to overwhelm the ecosystem natural aerosol dynamics, in a way that the diel variation of particle scattering and absorption is dominated by the boundary layer dynamics.

4.2 Particle mass scattering and absorption coefficients

Fine and coarse mode aerosol particle mass concentrations were obtained from the gravimetric analysis of 199 samples. The PM_{10} particle mass concentrations ranged between 5 and 25 $\mu g\,m^{-3}$ between February 2008 and April 2011, which is in accordance with previously reported values (e.g. Martin et al., 2010). Strong seasonal variations were observed in the ratio between PM_2 and PM_{10} particle mass concentrations, as a consequence of regional fires: in the wet season PM_2 accounted for 20–30 % of PM_{10}, whereas in the dry season the proportion increased to 40–80 % (Fig. 15). Therefore, from wet to dry season, the aerosol population changed to a particle number size distribution pattern that is more optically active, dominated by the fine mode.

ACPD
12, 23333–23401, 2012

This effect can be seen on mass scattering coefficients, calculated as the ratio between scattering coefficients at 550 nm and PM_{10} particle mass concentration (Fig. 16a). Average mass scattering coefficients increased from $0.9 \pm 0.5\,m^2\,g^{-1}$ in the wet season to $2.6 \pm 1.8\,m^2\,g^{-1}$ in the dry season. These values are in the range of previously reported mass scattering coefficients for the dry season Amazonian aerosols (Chand et al., 2006; Hobbs et al., 1997). To our knowledge, this is the first estimative of mass scattering coefficients for the wet season Amazonian aerosols, dominated by coarse mode biogenic particles. The mass absorption coefficient also showed a similar pattern (Fig. 16b), increasing from $0.09 \pm 0.07\,m^2\,g^{-1}$ to $0.27 \pm 0.24\,m^2\,g^{-1}$ from wet to dry season. Mass absorption coefficient for black carbon at 637 nm can be assumed $6.6\,m^2\,g^{-1}$ as in the MAAP (Müller et al., 2011b; Petzold et al., 2005), which implies that black carbon constitutes 5–10 % of the PM_{10} particle mass concentration in the dry season.

4.3 Relationships between scattering Ångström exponent, hemispheric backscattering ratio and particle size

In the literature, the scattering Ångström exponent and the backscatter ratio have been used as an indication of particle number size distribution. Particles with diameters around 0.1 µm, usually associated with urban pollution and biomass burning, have a steeper spectral dependency for scattering, and a smaller contribution to forward scattering in comparison to large particles typically associated with sea salt and mineral dust (e.g. Collaud Coen et al., 2007; Schuster et al., 2006). Therefore, both parameters are expected to decrease as the aerosol particle diameter increases.

The relationships with particle size were investigated through the comparison with the following weighted mean diameters calculated from sub micrometer aerosol particle number size distribution measurements (10–500 nm) taken between November 2009

ACPD
12, 23333–23401, 2012

and July 2010: the count mean diameter (CMD),

$$\mathrm{CMD} = \frac{\sum D_{\mathrm{P}_i} N_i}{N_{\mathrm{total}}} \tag{7}$$

the surface area mean diameter (SMD),

$$\mathrm{SMD} = \frac{\sum D_{\mathrm{P}_i} S_i}{S_{\mathrm{total}}} \tag{8}$$

and the volume mean diameter (VMD),

$$\mathrm{VMD} = \frac{\sum D_{\mathrm{P}_i} V_i}{V_{\mathrm{total}}} \tag{9}$$

where D_{P_i}, N_i, S_i, and V_i represents, respectively particle diameter, number concentration, surface area and volume of bin i; N_{total}, S_{total}, and V_{total} represents the corresponding parameters integrated for the whole diameter range. It is important to emphasize that scattering measurements refer to PM_7 particles, while the weighted mean diameters refer to sub micrometer particles. Occasionally, super micrometer particle number size distributions were available, but the dataset is not long enough to provide good statistics.

Figure 17 shows that the backscatter ratio at 550 nm was more sensitive to particle size than the Ångström exponent, particularly in the dry season. Similar relationships have been observed for the backscatter ratio at 450 and 700 nm. In accordance to that, Mie theory calculations performed by Collaud Coen et al. (2007) suggest that the backscatter fraction is more responsive to the smallest accumulation particles with less than 0.4 µm in diameter, while the Ångström exponent is more sensitive to particles with diameters between 0.5 and 0.8 µm. The same figure shows that the Ångström and the backscatter ratio decreased with SMD and VMD, as expected. Nevertheless, the dependency of the Ångström exponent with CMD contradicted the expectations,

ACPD
12, 23333–23401, 2012

increasing with particle size. This converse behavior has been reported for aerosols in a Chinese megacity (Garland et al., 2008) and in a boreal forest site (Virkkula et al., 2011). Schuster et al. (2006) argue that for bimodal aerosol particle number size distributions the Ångström exponent can decrease with particle size, depending on the ratio of fine and coarse particle concentration. The addition of coarse mode particles with spectrally flat extinctions reduces the overall spectral variability, decreasing the Ångström exponent and damping its sensitivity to the size of fine mode particles.

It is also clear on Fig. 17 that the data is more disperse during the wet season, due to the low aerosol concentrations. Higher dispersion of values in the wet season was also observed by Baars et al. (2012) for backscatter related Ångström exponents derived from LIDAR measurements at the same forest site. The range of values observed for the Ångström exponent and for the backscatter ratio in the dry season is enclosed in the range of values observed in the wet season. Therefore, it is difficult to use these optical parameters as a proxy for particle size or particle type in this Amazonian site, since their range of values does not help to distinguish the two main types of aerosols found in this site: biogenic and aged biomass burning particles.

4.4 Aerosol forcing efficiency

Daily averages of particle scattering, backscattering and absorption data were used to calculate the aerosol forcing efficiency at the top of the atmosphere, referring to the period between November 2009 and September 2010, when backscattering data was available. Figure 18 shows the histograms of aerosol forcing efficiency and cloud fraction for wet and dry season. The cloud cover was above 0.9 in 72 % of the wet season days, and in 46 % of the dry season days. As a consequence, the aerosol forcing efficiency was below $-3.5\,\mathrm{W\,m^{-2}}$ in 70 % of the wet season days and in 46 % of the dry season days. Therefore, in the wet season the radiative balance is dominated by the cloud cover, or, in other words, the radiative aerosol indirect effect predominates over the direct effect. In the dry season the radiative aerosol direct effect can be as

ACPD
12, 23333–23401, 2012

important as the indirect effect, at least referring to aged biomass burning particles. That may not be true for fresh biomass burning particles (e.g. Procopio et al., 2004).

It is not appropriate to present average values for variables with this kind of distribution. However, we present statistics for the aerosol forcing efficiency (Table 7) to have means of comparison with other studies. The average values shown in Table 7 agree with the range of 24 h forcing efficiencies of -8 to $-20\,W\,m^{-2}$ reported by Sena (2012) and references therein for the Amazon region. Note that the median values, which are more representative when one considers the distribution of forcing efficiencies, are about 10 times lower than the values reported in the literature, which are based on remote sensing data. That is because the aerosol forcing efficiencies calculated here included days with elevated cloud fractions, which is not feasible when dealing with remote sensing data. Within the period considered here, there were only 10 days with cloud fraction less than 0.1. Considering only those low cloud fraction days, the average forcing efficiency was $-46 \pm 9\,W\,m^{-2}$ for the wet season and $-51 \pm 10\,W\,m^{-2}$ for the dry season.

4.5 Optical closure study: iterative calculation of refractive indexes

An optical closure study was done for aerosol particle properties measured between 1 July–14 August 2009, period at which number size distribution measurements were available for particles in the optical diameter range of 10–6000 nm. Particle refractive index was calculated for each 60 min averaged number size distribution data, by means of matching calculated and measured particle scattering and absorption coefficients within 10 %. Both real and imaginary refractive indexes converged in 91 % of the hourly averaged data, whenever particle scattering, absorption and number size distributions were available.

In average, the model predicted 15 ± 5 % underestimation of 550 nm particle scattering coefficients due to the nephelometer angular truncation. This value is compatible with the correction factor calculated based on (Anderson and Ogren, 1998) (refer to Sect. 2.2). The modeled truncation correction factor varied between 8 % and 35 % at

ACPD
12, 23333–23401, 2012

550 nm. Correction factors above 30 % were obtained when the measured scattering coefficient at 550 nm was below 15 Mm^{-1}.

The average refractive index was (1.47 ± 0.07)–(0.008 ± 0.005) i, corresponding to effective values for aerosol particles in an Amazonian primary forest site in the dry season. The average particle refractive index obtained here is compatible with other estimative reported for Amazonia. Dubovik et al. (2002) report averages of 1.47–0.00093 i for the Amazon forest, retrieved from worldwide AERONET network of ground-based radiometers. Guyon et al., 2003 report averages of 1.42–0.006 i for background aerosols and of 1.41–0.013 i for biomass burning aerosol particles at a pasture site in Amazonia, under ambient RH conditions, using a similar procedure of closure between measured and calculated particle optical properties. Schkolnik et al. (2007) obtained 1.87–0.22 i for elemental carbon aerosols and 1.3 for organic aerosol, based on measurements of aerosol optical properties and chemical composition in an Amazonian pasture site during the dry season.

The closure between calculated and measured particle optical properties was not found in 9 % of the data for a variety of reasons: calculated scattering and absorption converged for different refractive indexes; particle volume concentration was not adequate to reach the measured scattering coefficient; or calculated absorption coefficient suffered a sudden increase as a function of the imaginary refractive index without convergence to measured values. This abrupt increase on calculated particle absorption occurred when measured absorption coefficients were in order of 0.1 Mm^{-1}. Improving the imaginary refractive index resolution from 0.0005 to 0.0001 did not help to increase the percentage of achieved closure between measured and modeled data.

It is worth to mention that the assumption of homogeneous spherical aerosols is a crude simplification for the variety of shapes and mixing states of atmospheric aerosol particles, especially when coarse mode particles are included. Several studies report the effects of non sphericity and different mixing states on aerosol optical properties (e.g. Cheng et al., 2006; Wagner et al., 2011; Ma et al., 2011), and this will be the focus of another paper.

ACPD
12, 23333–23401, 2012

To examine the scattering and absorption efficiency as a function of particle size, Mie model runs were performed using as input the previously converged refractive indexes. Each particle number size distribution starting at 10 nm was truncated at different particle diameters, comprising 13 particle size ranges (10–56; 10–115; 10–200; 10–300; 10–400; 10–500; 10–600; 10–750; 10–900; 10–1500; 10–2500; 10–4000; 10–6000 nm). The cumulative contribution of each particle size range to the scattering and absorption coefficients calculated for the entire size range (10–6000 nm) is shown Fig. 19. In average, particles with diameters between 10 and 500 nm accounted for 77 % of the scattering coefficient calculated for the entire size range. According to the model results, super micrometer particles contributed 50 % to the calculated absorption coefficients. This finding is associated with the assumption of size independent refractive indexes, and contradicts the expectative of decreasing absorption efficiency for particles larger than about 300 nm in diameter (Bond and Bergstrom, 2006). Nevertheless, the literature has shown evidences of the presence of light absorbing particles in the coarse mode. These particles are most likely of biogenic origin, since typical aerosol organic fractions in Amazonia range between 70 and 85 %, while soil dust particles comprise only 10–15 % of coarse particle mass concentration (Martin et al., 2010). Light absorbing carbonaceous aerosols of biogenic origin result from processes like oxidation of biogenic materials and polymerization, and are often denominated "brown carbon" (Andreae and Gelencsér, 2006; Andreae and Crutzen, 1997). Occurrence of external and internal mixing instead of the assumed homogeneous spherical aerosols might also have contributed to the increased importance of larger particles to the calculated absorption coefficients. Internal mixtures in the form of an absorbing core surrounded by a less absorbing shell increasing the absorption efficiency by a factor of 2–3 (Martins et al., 1998).

ACPD
12, 23333–23401, 2012

4.6 Influence of external sources over aerosol optical properties

4.6.1 Manaus urban plume influence

Between 2008 and 2011, 43 periods of influence of the Manaus urban plume over the measurement site were detected, comprising 1.5 % of the dataset. Episodes occurred with local winds ranging between 120 and 190°, and were characterized by a consistent increase on aerosol number concentrations, scattering and absorption coefficients. HYSPLIT back-trajectories were calculated for each episode, to derive the plume age and the number of trajectory points over the Manaus area (a square between the coordinates 2.95° S; 3.15° S; 59.85° W; 60.15° W). The plume age reaching the research site ranged between 5 and 24 h, and the trajectories enclosed 1 to 15 points inside the Manaus area. There was not a clear relationship between aerosol properties and the age of the urban plume, as shown in Fig. 20.

Table 8 shows statistics for aerosol particle properties measured during episodes of Manaus urban plume influence. Median particle scattering coefficients were 2.5 times greater than the ones measured at clean conditions during the wet season. Median particle absorption coefficients increased by a factor of 5 from samples taken under clean conditions to samples taken under the influence of the urban plume. Accordingly, the particle SSA decreased by 5 %.

Figure 21 shows an example of the Manaus plume effect over aerosol measurements at the forest reserve. Six air trajectories passing over the Manaus area reached the site between 04:00 and 09:00 LT of 25 April 2009. No precipitation occurred on this day. Under the influence of the urban plume, particle scattering coefficients increased by a factor of 1.7, absorption coefficients increased from 2 to 18 Mm^{-1}, particle number concentrations increased from 400 to 3300 cm^{-3}, and particle SSA values decreased from 0.93 to 0.75. After 09:00 LT, northeast winds predominated, bringing clean air and restoring the wet season typical particle number and mass concentrations.

ACPD
12, 23333–23401, 2012

4.6.2 Influence of African advection

Recent works reported the transport of African aerosols to the research site in the wet season of 2008 (e.g. Baars et al., 2011; Ben-Ami et al., 2010). The phenomenon might have occurred also in 2009 and 2010, but here only the well documented episodes occurred in 2008 (Table 4) will be used to calculate statistics for aerosol particle properties during the periods of influence of African aerosol advection. Table 9 shows that median particle absorption coefficients increased by factor of 2 when compared to the overall wet season statistics (Table 6). As a matter of comparison, Müller (2009) report particle absorption coefficients ranging from 0.1 to 10 Mm^{-1} for Saharan mineral dust in Southern Morocco. Particle scattering coefficients were not significantly affected by the advection of African aerosols, so that the SSA median values decreased by 7 % in comparison to the wet season values. The elevated number of hours of influence on particle measurements (~ 240 h in 4 months) attests the significance of this external source over Amazonian aerosol particle properties, especially during the wet season.

5 Conclusions

Two types of aerosol particles, with significantly different optical properties were identified in a pristine forest site in Amazonia: coarse mode predominant biogenic aerosols in the wet season (January–June), naturally released by the forest metabolism, and fine mode dominated biomass burning aerosols in the dry season (July–December), transported from regional fires. From wet to dry season, median aerosol particle scattering (550 nm) and absorption (637 nm) coefficients increased from 6.3 Mm^{-1} to 22 Mm^{-1}, and from 0.5 Mm^{-1} to 2.8 Mm^{-1}, respectively. On the other hand, the derived aerosol intrinsic properties, namely, the Ångström exponent for scattering, the backscatter ratio and the single scattering albedo, did not show a clear seasonal cycle. The median value for the dry particle SSA at 637 nm was 0.88 equally in the dry and in the wet season, and the values obtained are in accordance with AERONET SSA measurements

ACPD
12, 23333–23401, 2012

in the Amazon region. The weak seasonal variation of SSA, in spite of the increased concentrations of light absorbing biomass burning particles in the dry season, can be in part explained by the fact that both particle scattering and absorption increased by similar rates in the dry season. The particle scattering coefficients increased as a consequence of enhanced fine particle number and mass concentrations in the dry season (40–80 % of PM_{10} mass), which are more efficient to scatter light in comparison to the coarse mode dominated biogenic particles in the wet season. Accordingly, mass scattering coefficients at 550 nm increased from 0.9 ± 0.5 to $2.6 \pm 1.8\,g\,m^{-2}$ from wet to dry season. The corresponding increase on mass absorption coefficients at 637 nm was 0.09 ± 0.07 to $0.27 \pm 0.24\,g\,m^{-2}$. Another feature that contributed to the similarity of particle SSA values in wet and dry seasons was the advection of light absorbing aerosols from Africa, with recurring episodes between January and March.

There was a weak correlation between the scattering Ångström exponent and sub micrometer weighted mean diameters. The same holds for the backscatter ratio. As a result, it is not recommended to use these parameters as indicators of particle size in this Amazonian forest site, since their range of values does not help to distinguish between biogenic and biomass burning particles.

A closure between optical aerosol particle properties and number size distribution measurements was found in 91 % of the hourly averaged data between 1 July–14 August 2009. Particle refractive index was iteratively calculated, with an average value of (1.47 ± 0.07)–(0.008 ± 0.005) i. This is an effective value for the whole population of aerosol particles in an Amazonian primary forest site in the dry season. In average, particles with diameters between 10 and 500 nm accounted for 77 % of the scattering coefficient calculated for the entire size range.

Optical particle properties measured above the canopy were used to estimate the aerosol forcing efficiency at the top of the atmosphere. Results indicated that in this pristine forest site the radiative balance was dominated by cloud cover, or, in other words, the aerosol indirect effect predominated over the direct effect, particularly in the wet season. Due to the high cloud fractions, the aerosol forcing efficiency was be-

ACPD
12, 23333–23401, 2012

low $-3.5\,W\,m^{-2}$ in 70 % of the wet season days and in 46 % of the dry season days. Aerosol forcing efficiency median values are lower than the ones reported in the literature, which are based on remote sensing data. That is because the aerosol forcing efficiencies calculated here included days with elevated cloud fractions, which is not feasible when dealing with remote sensing data.

Besides the seasonal variation, the influence of external aerosol sources was observed occasionally. Between 2008 and 2011, 43 periods of influence of the Manaus urban plume were identified, comprising 1.5 % of the dataset. The events were characterized by a consistent increase on particle scattering (factor 2.5) and on absorption coefficients (factor 5), lasting from 4 h to a whole day. Advection of biomass burning and mineral dust particles from Africa affected 240 h of measurements between February and May 2008 (8 % of the corresponding dataset). The events lasted from 1 to 7 days, showing median particle absorption coefficients increased by factor of 2, and median SSA values decreased by 7 %, in comparison to wet season conditions.

Acknowledgements. This work was supported by Fundação de Amparo à Pesquisa do Estado de São Paulo (FAPESP – AEROCLIMA 08/58100-2), Conselho Nacional de Desenvolvimento Científico (CNPq) and European Integrated FP6 project on Aerosol Cloud Climate and Air Quality Interactions (EUCAARI – 34684), under the scope of LBA experiment. We thank INPA (Instituto Nacional de Pesquisas da Amazônia) for the coordination work of the LBA Experiment. We thank Ya Fang Cheng for providing a Mie code. We thank several key persons for the support on aerosol sampling and analysis: Alcides Ribeiro, Ana Lucia Loureiro, Fernando Morais, Fábio Jorge and Lívia Oliveira.

References

Anderson, T. L. and Ogren, J. A.: Determining aerosol radiative properties using the TSI 3563 integrating nephelometer, Aerosol Sci. Tech., 29, 57–69, doi:10.1080/02786829808965551, 1998.

Anderson, T. L., Covert, S. F., Marshall, S. F., Laucks, M. L., Charlson, R. J., Waggoner, A. P., Ogren, J. A., Caldow, R., Holm, R., Quant, F., Sem, G., Wiedensohler, A., Ahlquist, N.

ACPD

12, 23333–23401, 2012

A. and Bates, T. S.: Performance characteristics of a high-sensitivity, three wavelenght, total scatter/backscatter nephelometer, J. Atmos. Oceanic Technol., 13, 967–986, 1996.
Anderson, T. L., Covert, D. S., Wheeler, J. D., Harris, J., Perry, K. D., Trost, B. E., Jaffe, D. J., and Ogren, J. A.: Aerosol backscatter fraction and single scattering albedo, J. Geophys. Res., 104, 26793–26807, 1999.
Andreae, M. O.: Correlation between cloud condensation nuclei concentration and aerosol optical thickness in remote and polluted regions, Atmos. Chem. Phys., 9, 543–556, doi:10.5194/acp-9-543-2009, 2009.
Andreae, M. O. and Crutzen, P. J.: Atmospheric aerosols: biogeochemical sources and role in atmospheric chemistry, Science, 276, 1052, doi:10.1126/science.276.5315.1052, 1997.
Andreae, M. O. and Gelencsér, A.: Black carbon or brown carbon? The nature of light-absorbing carbonaceous aerosols, Atmos. Chem. Phys., 6, 3131–3148, doi:10.5194/acp-6-3131-2006, 2006.
Andreae, M. O., Rosenfeld, D., Artaxo, P., Costa, A. A., Frank, G. P., Longo, K. M., and Silva-Dias, M. A. F.: Smoking rain clouds over the Amazon, Science, 303, 1337–1342, doi:10.1126/science.1092779, 2004.
Andrews, E., Sheridan, P. J., Fiebig, M., McComiskey, A., Ogren, J. A., Arnott, P., Covert, D., Elleman, R., Gasparini, R., Collins, D., Jonsson, H., Schmid, B., and Wang, J.: Comparison of methods for deriving aerosol asymmetry parameter, J. Geophys. Res., 111, 1–16, doi:10.1029/2004JD005734, 2006.
Ångström, A.: On the atmospheric transmission of Sun radiation and on dust in the air, Geograf. Ann., 11, 156–166, 1929.
Ansmann, A., Baars, H., Tesche, M., Müller, D., Althausen, D., Engelmann, R., Pauliquevis, T., and Artaxo, P.: Dust and smoke transport from Africa to South America: lidar profiling over Cape Verde and the Amazon rainforest, Geophys. Res. Lett., 36, 2–6, doi:10.1029/2009GL037923, 2009.
Araújo, A. C., Nobre, A. D., Kruijt, B., Elbers, J. A., Dallarosa, R., Stefani, P., von Randow, C., Manzi, A. O., Culf, A. D., Gash, J. H. C., Valentini, R., and Kabat, P.: Comparative measurements of carbon dioxide fluxes from two nearby towers in a central Amazonian rainforest: the Manaus LBA site, J. Geophys. Res., 107, 8090, doi:10.1029/2001JD000676, 2002.
Artaxo, P. and Hansson, H.-C.: Size distribution of biogenic aerosol particles, Atmos. Environ., 29, 393–402, 1995.

ACPD
12, 23333–23401, 2012

Artaxo, P., Gerab, F., Yamasoe, M. A., and Martins, J. V.: Fine mode aerosol composition at three long-term atmospheric monitoring sites in the Amazon Basin, J. Geophys. Res., 99, 22857–22868, 1994.

Artaxo, P., Martins, J. V., Yamasoe, M. A., Procópio, A. S., Pauliquevis, T. M., Andreae, M. O., Guyon, P., Gatti, L. V., and Cordova, A. M. L.: Physical and chemical properties of aerosols in the wet and dry seasons in Rondônia, Amazonia, J. Geophys. Res., 107, 8081, doi:10.1029/2001JD000666, 2002.

Baars, H., Ansmann, A., Althausen, D., Engelmann, R., Artaxo, P., Pauliquevis, T., and Souza, R.: Further evidence for significant smoke transport from Africa to Amazonia, Geophys. Res. Lett., 38, 1–6, doi:10.1029/2011GL049200, 2011.

Ben-Ami, Y., Koren, I., Rudich, Y., Artaxo, P., Martin, S. T., and Andreae, M. O.: Transport of North African dust from the Bodélé depression to the Amazon Basin: a case study, Atmos. Chem. Phys., 10, 7533–7544, doi:10.5194/acp-10-7533-2010, 2010.

Bohren, C. F., Donald, R., and Huffman, D. R.: Absorption and scattering of light by small particles, John Wiley, Hoboken, NJ, USA, 1998.

Bond, T. and Bergstrom, R.: Light absorption by carbonaceous particles: an investigative review, Aerosol Sci. Tech., 40, 27–67, doi:10.1080/02786820500421521, 2006.

Chand, D., Guyon, P., Artaxo, P., Schmid, O., Frank, G. P., Rizzo, L. V., Mayol-Bracero, O. L., Gatti, L. V., and Andreae, M. O.: Optical and physical properties of aerosols in the boundary layer and free troposphere over the Amazon Basin during the biomass burning season, Atmos. Chem. Phys., 6, 2911–2925, doi:10.5194/acp-6-2911-2006, 2006.

Cheng, Y. F., Eichler, H., Wiedensohler, A., Heintzenberg, J., Zhang, Y. H., Hu, M., Herrmann, H., Zeng, L. M., Liu, S., Gnauk, T., Brüggemann, E., and He, L. Y.: Mixing state of elemental carbon and non-light-absorbing aerosol components derived from in situ particle optical properties at Xinken in Pearl River Delta of China, J. Geophys. Res., 111, 1–18, doi:10.1029/2005JD006929, 2006.

Cheng, Y. F., Wiedensohler, a., Eichler, H., Heintzenberg, J., Tesche, M., Ansmann, a., Wendisch, M., Su, H., Althausen, D., and Herrmann, H.: Relative humidity dependence of aerosol optical properties and direct radiative forcing in the surface boundary layer at Xinken in Pearl River Delta of China: an observation based numerical study, Atmos. Environ., 42, 6373–6397, doi:10.1016/j.atmosenv.2008.04.009, 2008.

ACPD

12, 23333–23401, 2012

Collaud Coen, M., Weingartner, E., Nyeki, S., Cozic, J., Henning, S., Verheggen, B., Gehrig, R., and Baltensperger, U.: Long-term trend analysis of aerosol variables at the high-alpine site Jungfraujoch, J. Geophys. Res., 112, D13213, doi:10.1029/2006JD007995, 2007.

Davidson, E. A., Artaxo, P., Balch, J. K., Brown, I. F., Bustamante, M. M. C., Arau, A. C. D., Coe, M. T., Defries, R. S., Keller, M., Longo, M., Munger, J. W., Schroeder, W., Soares-Filho, B. S., Souza Jr, C. M., and Wofsy, S. C.: The Amazon Basin in transition, Nature, 481, 321–328, doi:10.1038/nature10717, 2012.

Draxler, R. R. and Rolph, G.: HYbrid Single-Particle Lagrangian Integrated Trajectory Model, NOAA ARL, Boulder, CO, USA, available at: http://ready.arl.noaa.gov/HYSPLIT.php, 2012, last accesse: 5 March 2012.

Dubovik, O., Holben, B., Eck, T. F., Smirnov, A., Kaufman, Y. J., King, M. D., Tanré, D., and Slutsker, I.: Variability of absorption and optical properties of key aerosol types observed in worldwide locations, J. Atmos. Sci., 59, 590–608, 2002.

Fan, J., Zhang, R., Tao, W.-K., and Mohr, K. I.: Effects of aerosol optical properties on deep convective clouds and radiative forcing, J. Geophys. Res., 113, 1–16, doi:10.1029/2007JD009257, 2008.

Forster, P., Ramaswamy, V., Artaxo, P., Berntsen, T., Betts, R., Fahey, D. W., Haywood, J., Lean, J., Lowe, D. C., Myhre, G., Nganga, J., Prinn, R., Raga, G., Schulz, M., Van Dorland, R., Bodeker, G., Boucher, O., Collins, W.D., Conway, T.J., Dlugokencky, E., Elkins, J.W., Etheridge, D., Foukal, P., Fraser, P., Geller, M., Joos, F., Keeling, C. D., Kinne, S., Lassey, K., Lohmann, U., Manning, A.C., Montzka, S., Oram, D., O'Shaughnessy, K., Piper, S., Plattner, G.-K., Ponater, M., Ramankutty, N., Reid, G., Rind, D., Rosenlof, K., Sausen, R., Schwarzkopf, D., Solanki, S. K., Stenchikov, G., Stuber, N., Takemura, T., Textor, C., Wang, R., Weiss, R., and Whorf, T.: Changes in atmospheric constituents and in radiative forcing, in: Climate Change 2007: The Physical Science Basis, edited by: Solomon, S., Qin, D., Manning, M., Chen, Z., Marquis, M., Averyt, K. B., Tignor, M., and Miller, H. L., Cambridge University Press, Cambridge, United Kingdom and New York, USA, 2007

Garland, R. M., Yang, H., Schmid, O., Rose, D., Nowak, A., Achtert, P., Wiedensohler, A., Takegawa, N., Kita, K., Miyazaki, Y., Kondo, Y., Hu, M., Shao, M., Zeng, L. M., Zhang, Y. H., Andreae, M. O., and Pöschl, U.: Aerosol optical properties in a rural environment near the mega-city Guangzhou, China: implications for regional air pollution, radiative forcing and remote sensing, Atmos. Chem. Phys., 8, 5161–5186, doi:10.5194/acp-8-5161-2008, 2008.

ACPD
12, 23333–23401, 2012

Guyon, P., Boucher, O., Graham, B., Beck, J., Mayol-bracero, O. L., Roberts, G. C., Maenhaut, W., Artaxo, P., and Andreae, M. O.: Refractive index of aerosol particles over the Amazon tropical forest during LBA-EUSTACH 1999, J. Aerosol Sci., 34, 883–907, doi:10.1016/S0021-8502(03)00052-1, 2003.

Haerter, J. O., Roeckner, E., Tomassini, L., and von Storch, J.-S.: Parametric uncertainty effects on aerosol radiative forcing, Geophys. Res. Lett., 36, 1–5, doi:10.1029/2009GL039050, 2009.

Hansen, J., Sato, M., and Ruedy, R.: Radiative forcing and climate response, J. Geophys. Res., 102, 6831–6864, 1997.

Haywood, J. M. and Shine, K. P.: The effect of anthropogenic sulfate and soot aerosol on the clear sky planetary radiation budget, Geophys. Res. Lett., 22, 603–606, 1995.

Heim, M., Mullins, B., Umhauer, H., and Kasper, G.: Performance evaluation of three optical particle counters with an efficient "multimodal" calibration method, J. Aerosol Sci., 39, 1019–1031, doi:10.1016/j.jaerosci.2008.07.006, 2008.

Hinds, W. C.: Aerosol Technology, Wiley – Interscience, New York, NY, USA, 1999.

Hobbs, P. V., Reid, J. S., Kotchenruther, R. A., Ferek, R. J., and Weiss, R.: Direct radiative forcing by smoke from biomass burning, Science, 275, 1777–1778, doi:10.1126/science.275.5307.1777, 1997.

Holben, B. N., Eck, T. F., Slutsker, I., Smirnov, A., Sinyuk, A., Schafer, J., Giles, D., and Dubovik, O.: Aeronet's version 2.0 quality assurance criteria, NASA's Goddard Space Flight Center, Greebelt, USA, available at: http://aeronet.gsfc.nasa.gov/newweb/PDF/AERONETcriteriafinal1.pdf, last access: 23 April 2012, 2006.

Hudson, J. G. and Yum, S. S.: Cloud condensation nuclei spectra and polluted and clean clouds over the Indian Ocean, J. Geophys. Res., 107, 8022, doi:10.1029/2001JD000829, 2002.

Hulstrom, R., Bird, R., and Riordan, C.: Spectral solar irradiance data sets for selected terrestrial conditions, Solar Cells, 15, 365–391, 1985.

IBGE: Estimativa Populacional, Instituto Brasileiro de Geografia e Estatistica, Rio de Janeiro, Brazil, available at: www.ibge.gov.br/home/estatistica/populacao/estimativa2011, last access: 20 May 2012, 2011.

Kaufman, Y., Hobbs, P., Kirchhoff, V., Artaxo, P., Remer, L. A., Holben, B. N., King, M. D., Ward, D. E., Prins, E. M., Longo, K. M., Mattos, L. F., Nobre, C. A., Spinhirne, J. D., Ji, Q., Thompson, A. M., Gleason, J. F., Christopher, S. A., and Tsay, S. C.: Smoke, clouds, and radiation-Brazil (SCAR-B) experiment, J. Geophys. Res., 103, 31783–31808, 1998.

ACPD
12, 23333–23401, 2012

Kaufman, Y. J., Koren, I., Remer, L. A., Tanré, D., Ginoux, P., and Fan, S.: Dust transport and deposition observed from the Terra-Moderate Resolution Imaging Spectroradiometer (MODIS) spacecraft over the Atlantic Ocean, J. Geophys. Res., 110, 1–16, doi:10.1029/2003JD004436, 2005.

Komppula, M., Lihavainen, H., Kerminen, V. M., Kulmala, M., and Viisanen, Y.: Measurements of cloud droplet activation of aerosol particles at a clean subarctic background site, J. Geophys. Res., 110, D06204, doi:10.1029/2004JD005200, 2005.

Koren, I., Kaufman, Y. J., Remer, L. A., and Martins, J. V.: Measurement of the effect of Amazon smoke on inhibition of cloud formation, Science, 303, 1342, doi:10.1126/science.1089424, 2004.

Kotchenruther, R. A. and Hobbs, P. V.: Humidification factors of aerosols from biomass burning in Brazil, J. Geophys. Res., 103, 32081–32089, 1998.

Kulmala, M., Asmi, A., Lappalainen, H. K., Baltensperger, U., Brenguier, J.-L., Facchini, M. C., Hansson, H.-C., Hov, Ø., O'Dowd, C. D., Pöschl, U., Wiedensohler, A., Boers, R., Boucher, O., de Leeuw, G., Denier van der Gon, H. A. C., Feichter, J., Krejci, R., Laj, P., Lihavainen, H., Lohmann, U., McFiggans, G., Mentel, T., Pilinis, C., Riipinen, I., Schulz, M., Stohl, A., Swietlicki, E., Vignati, E., Alves, C., Amann, M., Ammann, M., Arabas, S., Artaxo, P., Baars, H., Beddows, D. C. S., Bergström, R., Beukes, J. P., Bilde, M., Burkhart, J. F., Canonaco, F., Clegg, S. L., Coe, H., Crumeyrolle, S., D'Anna, B., Decesari, S., Gilardoni, S., Fischer, M., Fjaeraa, A. M., Fountoukis, C., George, C., Gomes, L., Halloran, P., Hamburger, T., Harrison, R. M., Herrmann, H., Hoffmann, T., Hoose, C., Hu, M., Hyvärinen, A., Hõrrak, U., Iinuma, Y., Iversen, T., Josipovic, M., Kanakidou, M., Kiendler-Scharr, A., Kirkevåg, A., Kiss, G., Klimont, Z., Kolmonen, P., Komppula, M., Kristjánsson, J.-E., Laakso, L., Laaksonen, A., Labonnote, L., Lanz, V. A., Lehtinen, K. E. J., Rizzo, L. V., Makkonen, R., Manninen, H. E., McMeeking, G., Merikanto, J., Minikin, A., Mirme, S., Morgan, W. T., Nemitz, E., O'Donnell, D., Panwar, T. S., Pawlowska, H., Petzold, A., Pienaar, J. J., Pio, C., Plass-Duelmer, C., Prévôt, A. S. H., Pryor, S., Reddington, C. L., Roberts, G., Rosenfeld, D., Schwarz, J., Seland, Ø., Sellegri, K., Shen, X. J., Shiraiwa, M., Siebert, H., Sierau, B., Simpson, D., Sun, J. Y., Topping, D., Tunved, P., Vaattovaara, P., Vakkari, V., Veefkind, J. P., Visschedijk, A., Vuollekoski, H., Vuolo, R., Wehner, B., Wildt, J., Woodward, S., Worsnop, D. R., van Zadelhoff, G.-J., Zardini, A. A., Zhang, K., van Zyl, P. G., Kerminen, V.-M., S Carslaw, K., and Pandis, S. N.: General overview: European Integrated project on Aerosol Cloud Climate and Air Quality interactions (EUCAARI) – integrat-

ACPD
12, 23333–23401, 2012

ing aerosol research from nano to global scales, Atmos. Chem. Phys., 11, 13061–13143, doi:10.5194/acp-11-13061-2011, 2011.
Lewis, S. L., Brando, P. M., Phillips, O. L., van der Heijden, G. M. F., and Nepstad, D.: The 2010 Amazon drought, Science, 331, 554, doi:10.1126/science.1200807, 2011.
Liu, Y. and Daum, P.: The effect of refractive index on size distributions and light scattering coefficients derived from optical particle counters, J. Aerosol Sci., 31, 945–957, doi:10.1016/S0021-8502(99)00573-X, 2000.
Loeb, N. G. and Su, W.: Direct aerosol radiative forcing uncertainty based on a radiative perturbation analysis, J. Climate, 23, 5288–5293, doi:10.1175/2010JCLI3543.1, 2010.
Ma, N., Zhao, C. S., Nowak, A., Müller, T., Pfeifer, S., Cheng, Y. F., Deng, Z. Z., Liu, P. F., Xu, W. Y., Ran, L., Yan, P., Göbel, T., Hallbauer, E., Mildenberger, K., Henning, S., Yu, J., Chen, L. L., Zhou, X. J., Stratmann, F., and Wiedensohler, A.: Aerosol optical properties in the North China Plain during HaChi campaign: an in-situ optical closure study, Atmos. Chem. Phys., 11, 5959–5973, doi:10.5194/acp-11-5959-2011, 2011.
Martin, S. T., Andreae, M. O., Althausen, D., Artaxo, P., Baars, H., Borrmann, S., Chen, Q., Farmer, D. K., Guenther, A., Gunthe, S. S., Jimenez, J. L., Karl, T., Longo, K., Manzi, A., Müller, T., Pauliquevis, T., Petters, M. D., Prenni, A. J., Pöschl, U., Rizzo, L. V., Schneider, J., Smith, J. N., Swietlicki, E., Tota, J., Wang, J., Wiedensohler, A., and Zorn, S. R.: An overview of the Amazonian Aerosol Characterization Experiment 2008 (AMAZE-08), Atmos. Chem. Phys., 10, 11415–11438, doi:10.5194/acp-10-11415-2010, 2010a.
Martin, S. T., Andreae, M. O., Artaxo, P., Baumgardner, D., Chen, Q., Goldstein, A. H., Guenther, A., Heald, C. L., Bracero, O. L. M., Mcmurry, P. H., Pauliquevis, T., Pöschl, U., Prather, K. A., Roberts, G. C., Saleska, S. R., Silva-Dias, M. A., Spracklen, D. V., Swietlicki, E., and Trebs, I.: Sources and properties of Amazonian aerosol particles, Rev. Geophys., 48, RG2002, doi:10.1029/2008RG000280, 2010b.
Martins, J. V., Artaxo, P., Liousse, C., Reid, J. S., Hobbs, P. V., and Kaufman, Y. J.: Effects of black carbon content, particle size, and mixing on light absorption by aerosols from biomass burning in Brazil, J. Geophys. Res., 103, 41–50, 1998.
Müller, T., Schladitz, A., Massling, A., Kaaden, N., Kandler, K., and Wiedensohler, A.: Spectral absorption coefficients and imaginary parts of refractive indices of Saharan dust during SAMUM-1, Tellus B, 61, 79–95, doi:10.1111/j.1600-0889.2008.00399.x, 2009.
Müller, T., Henzing, J. S., de Leeuw, G., Wiedensohler, A., Alastuey, A., Angelov, H., Bizjak, M., Collaud Coen, M., Engström, J. E., Gruening, C., Hillamo, R., Hoffer, A., Imre, K., Ivanow, P.,

ACPD
12, 23333–23401, 2012

Jennings, G., Sun, J. Y., Kalivitis, N., Karlsson, H., Komppula, M., Laj, P., Li, S.-M., Lunder, C., Marinoni, A., Martins dos Santos, S., Moerman, M., Nowak, A., Ogren, J. A., Petzold, A., Pichon, J. M., Rodriquez, S., Sharma, S., Sheridan, P. J., Teinilä, K., Tuch, T., Viana, M., Virkkula, A., Weingartner, E., Wilhelm, R., and Wang, Y. Q.: Characterization and intercomparison of aerosol absorption photometers: result of two intercomparison workshops, Atmos. Meas. Tech., 4, 245–268, doi:10.5194/amt-4-245-2011, 2011.

Nessler, R., Weingartner, E., and Baltensperger, U.: Effect of humidity on aerosol light absorption and its implications for extinction and the single scattering albedo illustrated for a site in the lower free troposphere, J. Aerosol Sci., 36, 958–972, doi:10.1016/j.jaerosci.2004.11.012, 2005.

Petzold, A., Schloesser, H., Sheridan, P., Arnott, W. P., Ogren, J., and Virkkula, A.: Evaluation of multiangle absorption photometry for measuring aerosol light absorption, Aerosol Sci. Tech., 39, 40–51, doi:10.1080/027868290901945, 2005.

Prenni, A. J., Petters, M. D., Kreidenweis, S. M., Heald, C. L., Martin, S. T., Artaxo, P., Garland, R. M., Wollny, A. G., and Pöschl, U.: Relative roles of biogenic emissions and Saharan dust as ice nuclei in the Amazon Basin, Nat. Geosci., 2, 402–405, doi:10.1038/ngeo517, 2009.

Procopio, A. S., Artaxo, P., Kaufman, Y. J., Remer, L. A., Schafer, J. S., and Holben, B. N.: Multiyear analysis of Amazonian biomass burning smoke radiative forcing of climate, Geophys. Res. Lett., 31, L03108, doi:10.1029/2003GL018646, 2004.

Rissler, J., Vestin, A., Swietlicki, E., Fisch, G., Zhou, J., Artaxo, P., and Andreae, M. O.: Size distribution and hygroscopic properties of aerosol particles from dry-season biomass burning in Amazonia, Atmos. Chem. Phys., 6, 471–491, doi:10.5194/acp-6-471-2006, 2006.

Rizzo, L. V., Correia, A. L., Artaxo, P., Procópio, A. S., and Andreae, M. O.: Spectral dependence of aerosol light absorption over the Amazon Basin, Atmos. Chem. Phys., 11, 8899–8912, doi:10.5194/acp-11-8899-2011, 2011.

Rolph, G. D.: Real-time Environmental Applications and Display sYstem (READY) Website, NOAA Air Resources Laboratory, Silver Spring, MD, available at: http://ready.arl.noaa.gov, last access: 5 June 2012, 2012.

Schafer, J. S., Eck, T. F., Holben, B. N., Artaxo, P. and Duarte, A. F.: Characterization of the optical properties of atmospheric aerosols in Amazônia from long-term AERONET monitoring (1993–1995 and 1999–2006), J. Geophys. Res., 113, 1–16, doi:10.1029/2007JD009319, 2008.

ACPD
12, 23333–23401, 2012

Schkolnik, G., Chand, D., Hoffer, A., Andreae, M., Erlick, C., Swietlicki, E., and Rudich, Y.: Constraining the density and complex refractive index of elemental and organic carbon in biomass burning aerosol using optical and chemical measurements, Atmos. Environ., 41, 1107–1118, doi:10.1016/j.atmosenv.2006.09.035, 2007.

Schuster, G. L., Dubovik, O., and Holben, B. N.: Angstrom exponent and bimodal aerosol size distributions, J. Geophys. Res., 111, 1–14, doi:10.1029/2005JD006328, 2006.

Sena, E. T., Artaxo, P., and Correia, A. L.: The impact of deforestation in the Amazonian atmospheric radiative balance: a remote sensing assessment, Atmos. Chem. Phys. Discuss., 12, 14837–14874, doi:10.5194/acpd-12-14837-2012, 2012.

Sheridan, P. J., Jefferson, A., and Ogren, J. A.: Spatial variability of submicrometer aerosol radiative properties over the Indian Ocean during INDOEX, J. Geophys. Res., 107, 1–17, 2002.

Shindell, D. and Faluvegi, G.: Climate response to regional radiative forcing during the twentieth century, Nat. Geosci., 2, 294–300, doi:10.1038/ngeo473, 2009.

Tuch, T. M., Haudek, A., Müller, T., Nowak, A., Wex, H., and Wiedensohler, A.: Design and performance of an automatic regenerating adsorption aerosol dryer for continuous operation at monitoring sites, Atmos. Meas. Tech., 2, 417–422, doi:10.5194/amt-2-417-2009, 2009.

Virkkula, A., Backman, J., Aalto, P. P., Hulkkonen, M., Riuttanen, L., Nieminen, T., dal Maso, M., Sogacheva, L., de Leeuw, G., and Kulmala, M.: Seasonal cycle, size dependencies, and source analyses of aerosol optical properties at the SMEAR II measurement station in Hyytiälä, Finland, Atmos. Chem. Phys., 11, 4445–4468, doi:10.5194/acp-11-4445-2011, 2011.

Wagner, R., Kandler, K., Linke, C., Muller, T., and Schnaiter, M.: Shape dependency of the extinction and absorption cross sections of dus aerosols modeled as randomly oriented spheroids, AAPP – Atti della Accademia Peloritana dei Pericolanti, Classe di Scienze Fisiche, Matematiche e Naturali, 89, 1–4, doi:10.1478/C1V89S1P094, 2011.

Wiedensohler, A., Birmili, W., Nowak, A., Sonntag, A., Weinhold, K., Merkel, M., Wehner, B., Tuch, T., Pfeifer, S., Fiebig, M., Fjäraa, A. M., Asmi, E., Sellegri, K., Depuy, R., Venzac, H., Villani, P., Laj, P., Aalto, P., Ogren, J. A., Swietlicki, E., Williams, P., Roldin, P., Quincey, P., Hüglin, C., Fierz-Schmidhauser, R., Gysel, M., Weingartner, E., Riccobono, F., Santos, S., Grüning, C., Faloon, K., Beddows, D., Harrison, R., Monahan, C., Jennings, S. G., O'Dowd, C. D., Marinoni, A., Horn, H.-G., Keck, L., Jiang, J., Scheckman, J., McMurry, P. H., Deng, Z., Zhao, C. S., Moerman, M., Henzing, B., de Leeuw, G., Löschau, G., and Bas-

ACPD
12, 23333–23401, 2012

tian, S.: Mobility particle size spectrometers: harmonization of technical standards and data structure to facilitate high quality long-term observations of atmospheric particle number size distributions, Atmos. Meas. Tech., 5, 657–685, doi:10.5194/amt-5-657-2012, 2012.

Zhou, J., Swietlicki, E., Hansson, H. C., and Artaxo, P.: Submicrometer aerosol particle size distribution and hygroscopic growth measured in the Amazon rain forest during the wet season, J. Geohpys. Res., 107, D20, doi:10.1029/2000JD000203, 2002.

ACPD

12, 23333–23401, 2012

Table 1. Uncertainties ($\delta\sigma_s$) estimated for 30 min averaging periods for scattering coefficients (σ_s) ranging between 1 and 100 Mm^{-1}, for sub micrometer and super micrometer aerosol particles. Relative errors are shown in brackets.

	Sub micrometer particles			Super micrometer particles		
σ_s Mm^{-1}	$\delta\sigma_s(450)$ Mm^{-1}	$\delta\sigma_s(550)$ Mm^{-1}	$\delta\sigma_s(700)$ Mm^{-1}	$\delta\sigma_s(450)$ Mm^{-1}	$\delta\sigma_s(550)$ Mm^{-1}	$\delta\sigma_s(700)$ Mm^{-1}
1	0.27 (27 %)	0.20 (20 %)	0.14 (14 %)	0.39 (39 %)	0.34 (34 %)	0.31 (31 %)
10	0.80 (8 %)	0.77 (8 %)	0.78 (8 %)	2.90 (29 %)	2.90 (29 %)	2.90 (29 %)
100	7.6 (8 %)	7.5 (7 %)	7.7 (8 %)	28.9 (29 %)	28.9 (29 %)	28.9 (29 %)

ACPD
12, 23333–23401, 2012

Table 2. Uncertainties ($\delta\sigma_{bs}$) estimated for 30 min averaging periods for backscattering coefficients (σ_{bs}) ranging between 0.1 and 10 Mm^{-1}, for sub micrometer and super micrometer aerosol particles. Relative errors are shown in brackets.

	Sub micrometer particles			Super micrometer particles		
σ_{bs} Mm^{-1}	$\delta\sigma_{bs}(450)$ Mm^{-1}	$\delta\sigma_{bs}(550)$ Mm^{-1}	$\delta\sigma_{bs}(700)$ Mm^{-1}	$\delta\sigma_{bs}(450)$ Mm^{-1}	$\delta\sigma_{bs}(550)$ Mm^{-1}	$\delta\sigma_{bs}(700)$ Mm^{-1}
0.1	0.23 (230 %)	0.10 (100 %)	0.17 (170 %)	0.23 (230 %)	0.10 (100 %)	0.17 (170 %)
1	0.24 (24 %)	0.13 (13 %)	0.18 (18 %)	0.24 (24 %)	0.13 (13 %)	0.19 (19 %)
10	0.76 (8 %)	0.7 (7 %)	0.8 (8 %)	0.89 (9 %)	0.9 (9 %)	0.9 (9 %)

ACPD
12, 23333–23401, 2012

Table 3. Fire spots detected during the dry season (July–December) in the Amazonas State, Pará State, Legal Amazonia area, forest reserve neighbor municipalities (Manaus, Rio Preto da Eva, Presidente Figueiredo, Novo Airão), and municipalities eastern to the forest reserve in the State of Amazonas (Barreirinha, Itapiranga, Manaus, Nhamundá, Parintins, São Sebastião do Uatumã, Silves and Urucará). Source: CPTEC/INPE.

	Amazonas State	Pará State	Legal Amazonia	Neighbor districts	Eastern districts
Dry 2008	11 038	103 833	346 983	112	269
Dry 2009	14 576	103 265	246 513	813	2244
Dry 2010	20 613	164 618	686 670	367	1023

ACPD
12, 23333–23401, 2012

Table 4. Periods of influence of African particle advection from February to May 2008, reported by Baars et al. (2011).

Period of influence	Aerosol type
25 Feb–1 Mar 2008	Smoke + dust
15–16 Mar 2008	Smoke + dust
8 Apr 2008	Smoke + dust
8–11 May 2008	Mostly dust

ACPD
12, 23333–23401, 2012

Table 5. Year to year and seasonal variability on aerosol particle scattering and absorption. The percent data coverage is also shown.

	Aerosol scattering 550 nm (Mm^{-1})				Aerosol absorption 637 nm (Mm^{-1})			
	median	1st quartile	3rd quartile	coverage	median	1st quartile	3rd quartile	coverage
Dry 2008	15	11	21	36.4 %	1.86	1.13	2.92	51.1 %
Dry 2009	35	19	61	98.9 %	3.69	2.06	6.07	95.1 %
Dry 2010	16	9.2	32	84.8 %	3.00	1.15	5.62	98.4 %
Wet 2008	5.5	2.8	9.3	59.9 %	0.34	0.16	0.80	59.3 %
Wet 2009	8.1	4.6	14	58.6 %	0.41	0.22	0.88	85.6 %
Wet 2010	7.5	4.7	12	82.3 %	0.95	0.34	2.22	84.0 %
Wet 2011	3.9	2.1	6.6	51.1 %	0.37	0.17	0.79	67.0 %

ACPD
12, 23333–23401, 2012

Table 6. Average, standard deviation, 25th, 50th and 75th percentiles, and number of observations for aerosol particle scattering coefficients (σ_s) and backscatter ratios (b) at 450, 550 and 700 nm, absorption coefficients (σ_a) at 637 nm, Ångström exponent for scattering ($\mathring{a}_{450-700}$) and single scattering albedo at 637 nm (ω_0), based on 30 min averages.

		Avg ± stdev	Percentiles 25	50	75	N
σ_s (450) Mm^{-1}	Wet season	11 ± 9	4.7	8.3	14	19 155
	Dry season	50 ± 64	17	31	59	17 581
	All data	29 ± 49	7.3	15	31	36 736
σ_s (550) Mm^{-1}	Wet season	8.1 ± 7.2	3.4	6.3	11	19 155
	Dry season	36 ± 48	12	22	42	17 581
	All data	21 ± 36	5.4	11	23	36 736
σ_s (700) Mm^{-1}	Wet season	5.4 ± 5.1	2.3	4.2	7.0	19 155
	Dry season	18 ± 23	7.0	11	20	17 581
	All data	11 ± 17	3.4	6.5	12	36 736
b (450)	Wet season	0.13 ± 0.05	0.11	0.13	0.15	6571
	Dry season	0.13 ± 0.02	0.12	0.13	0.14	4751
	All data	0.13 ± 0.04	0.11	0.13	0.14	11 322
b (550)	Wet season	0.15 ± 0.05	0.13	0.15	0.17	6571
	Dry season	0.15 ± 0.03	0.14	0.15	0.17	4751
	All data	0.15 ± 0.04	0.13	0.15	0.17	11 322
b (700)	Wet season	0.20 ± 0.07	0.16	0.19	0.22	6571
	Dry season	0.20 ± 0.04	0.18	0.20	0.22	4751
	All data	0.20 ± 0.06	0.17	0.20	0.22	11 322
σ_a (637) Mm^{-1}	Wet season	1.0 ± 1.4	0.2	0.5	1.1	24 158
	Dry season	3.9 ± 3.6	1.4	2.8	5.2	19 567
	All data	2.3 ± 3.0	0.4	1.1	3.0	43 725
$\mathring{a}_{450-700}$	Wet season	1.48 ± 1.12	1.02	1.40	1.80	19 155
	Dry season	1.70 ± 0.41	1.43	1.73	1.98	17 581
	All data	1.59 ± 0.86	1.22	1.58	1.92	36 736
ω_0 (637)	Wet season	0.86 ± 0.09	0.81	0.88	0.93	15 283
	Dry season	0.87 ± 0.06	0.84	0.88	0.91	15 766
	All data	0.86 ± 0.08	0.83	0.88	0.91	31 049

ACPD
12, 23333–23401, 2012

Table 7. Statistics for aerosol forcing efficiency at the top of the atmosphere calculated based on daily averages of scattering, backscatter ratio, absorption and cloud fraction (MODIS), enclosing the period between November 2009 and September 2010.

	Aerosol forcing efficiency $\Delta F/\mathrm{AOD}$ ($\mathrm{W\,m^{-2}}$)					
	Average	Standard deviation	Median	1st quartile	3rd quartile	coverage
All data	−9	15	−0.8	−13	0.0	65 %
Wet season	−6	13	−0.3	−6	0.0	76 %
Dry season	−13	19	−6	−23	−0.2	55 %

ACPD
12, 23333–23401, 2012

Table 8. Statistics for aerosol particle scattering coefficients (550 nm), scattering Ångström exponent, absorption coefficient (637 nm), single scattering albedo (637 nm) and particle number concentration during episodes of influence of the Manaus urban plume between February 2008 and June 2011.

	Scattering (Mm^{-1})	Ångström	Absorption (Mm^{-1})	SSA	Concentration (cm^{-3})
Median	16.0	1.72	2.68	0.84	1502
1st quartile	12.2	1.41	1.51	0.78	1026
3rd quartile	22.3	2.00	4.96	0.89	2269
Number of hours of measurements affected (2008–2011)	223	223	213	211	158

ACPD
12, 23333–23401, 2012

Table 9. Statistics for aerosol particle scattering coefficients (550 nm), scattering Ångström exponent, absorption coefficient (637 nm), single scattering albedo (637 nm) and particle number concentration during episodes of African advection between February and May 2008.

	Scattering (Mm^{-1})	Ångström	Absorption (Mm^{-1})	SSA	Concentration (cm^{-3})
Median	6.2	1.29	0.95	0.82	352
1st quartile	3.3	0.88	0.38	0.77	300
3rd quartile	12.0	1.50	1.46	0.94	488
Number of hours of measurements affected in 2008	254	254	240	230	202

ACPD
12, 23333–23401, 2012

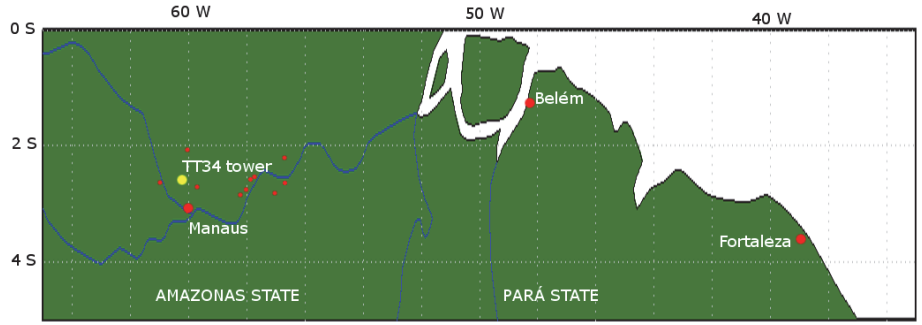

Fig. 1. The yellow circle marks the location of the TT34 measurement tower in the Sate of Amazonas, Brazil. The big red circles mark the position of some of the major cities in the Brazilian North and Northeast regions (more than 1.4 million inhabitants each). The small red circles mark the position of municipalities neighbor to the forest reserve (Rio Preto da Eva, Presidente Figueiredo, Novo Airão), and municipalities eastern to the forest reserve in the State of Amazonas (Barreirinha, Itapiranga, Nhamundá, Parintins, São Sebastião do Uatumã, Silves and Urucará).

ACPD
12, 23333–23401, 2012

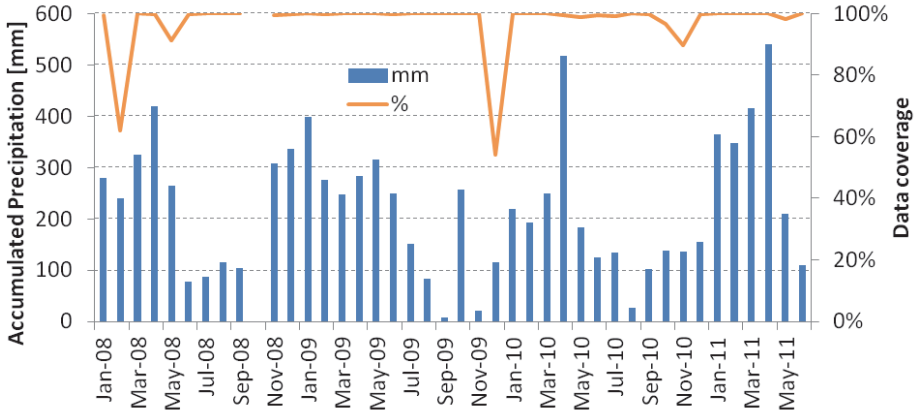

Fig. 2. Monthly accumulated precipitation measured at INPA's K34 tower from January 2008 to June 2011. The line represents the percent data coverage for each month.

ACPD
12, 23333–23401, 2012

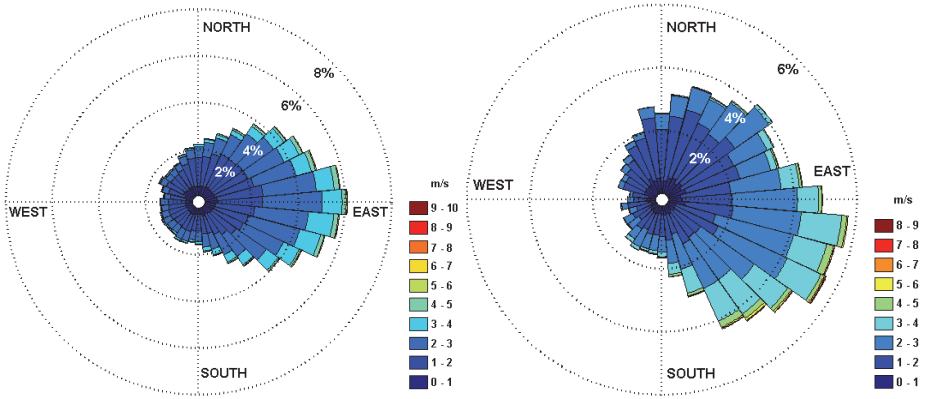

Fig. 3. (a) Wind rose plots for the period between January 2008 and June2011. **(b)** Wind rose for the months of June and July, from 2008 to 2011. The Manaus city is located 60 km away in the southeast direction.

ACPD
12, 23333–23401, 2012

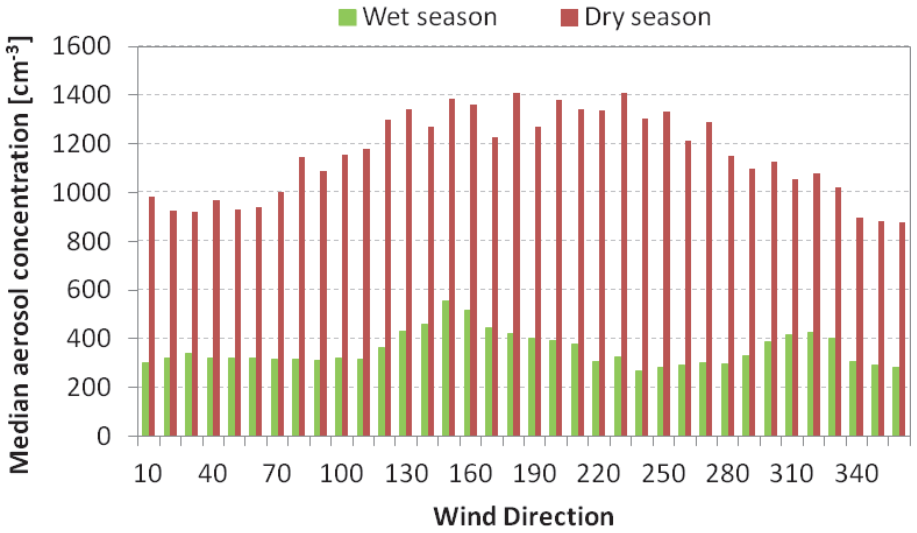

Fig. 4. Median aerosol particle number concentration as a function of wind direction for the wet season (January–June) and for the dry season (July–December).

ACPD
12, 23333–23401, 2012

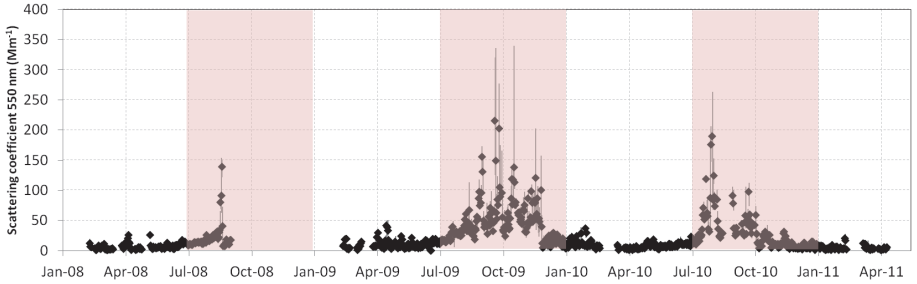

Fig. 5. Daily medians of aerosol particle scattering coefficients at 550 nm, from February 2008 to May 2011. Error bars represent first and third quartiles. Shaded areas represent the dry season period.

ACPD
12, 23333–23401, 2012

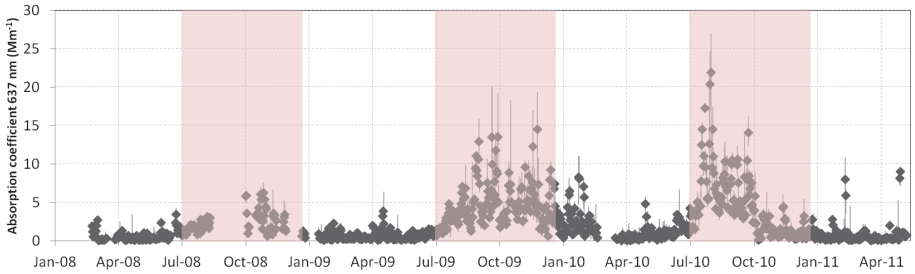

Fig. 6. Daily medians of aerosol particle absorption coefficients, from February 2008 to May 2011. Error bars represent first and third quartiles. Shaded areas represent the dry season period.

ACPD
12, 23333–23401, 2012

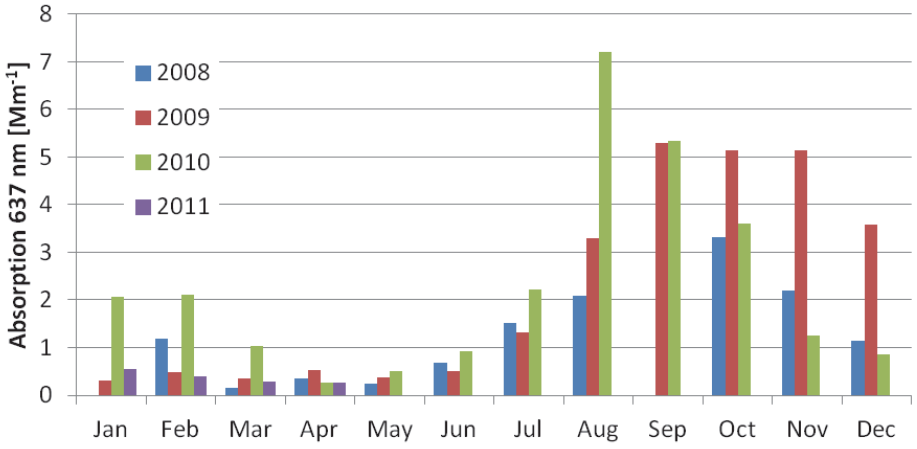

Fig. 7. Monthly medians of aerosol particle absorption coefficients at 637 nm.

ACPD
12, 23333–23401, 2012

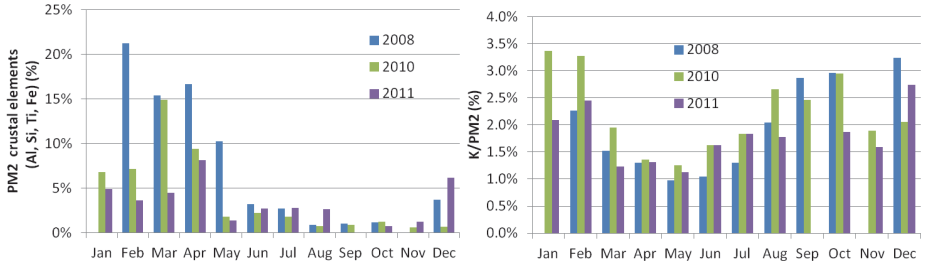

Fig. 8. Percentage of crustal elements (Al, Si, Ti, Fe) and potassium with respect to the fine mode aerosol particle mass (PM_2).

ACPD
12, 23333–23401, 2012

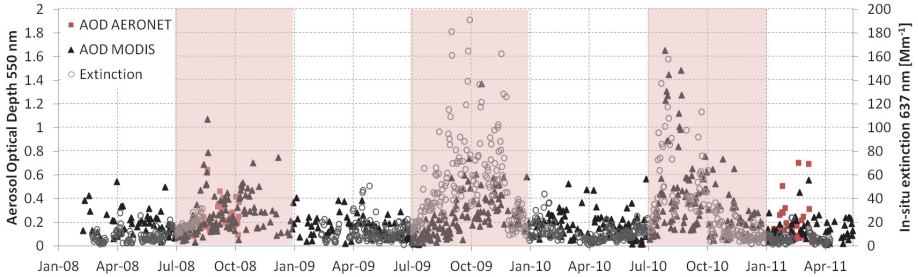

Fig. 9. Daily averages of aerosol optical depth (AOD) observations from MODIS (TERRA-AQUA), AERONET (Manaus) and in situ extinction measurements above the canopy. AOD observations from MODIS were integrated inside an area with 40 km radius around the in situ measurement site. AOD observations from AERONET are level 2.0 in 2008 July–October and level 1.5 in 2011 January–April, and were interpolated to 550 nm using AOD(500) and the Ångström exponent between 440 and 675 nm. Shaded areas represent the dry season period.

ACPD
12, 23333–23401, 2012

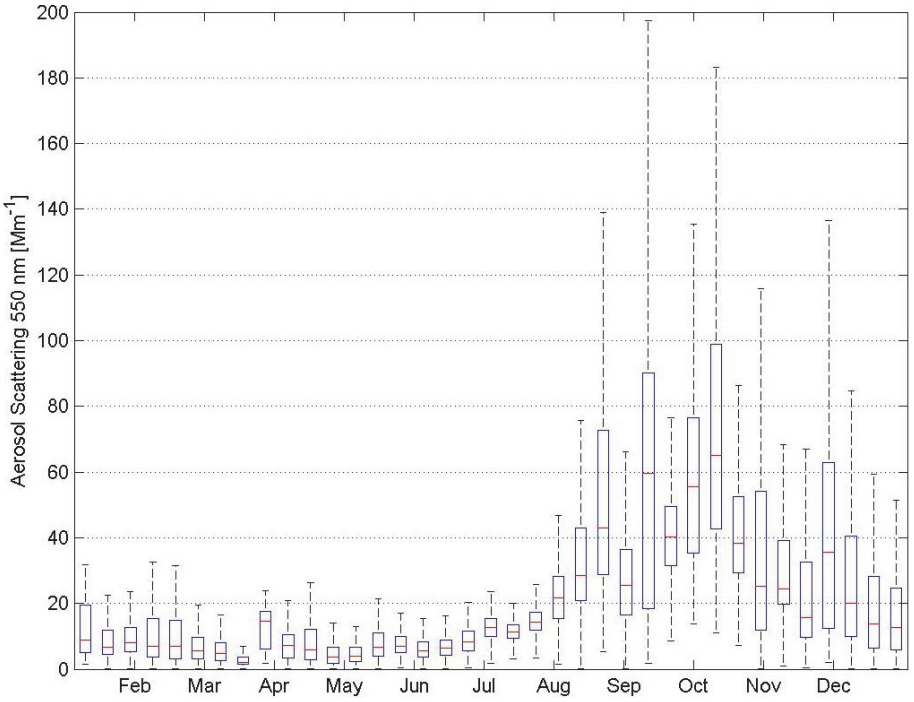

Fig. 10. Box plot considering particle scattering coefficients at 550 nm between February 2008 and May 2011. Statistics were calculated for each 10 Julian days. The box lines represent the lower quartile, median, and upper quartile values. Whiskers extend within 1.5 times the interquartile range.

ACPD
12, 23333–23401, 2012

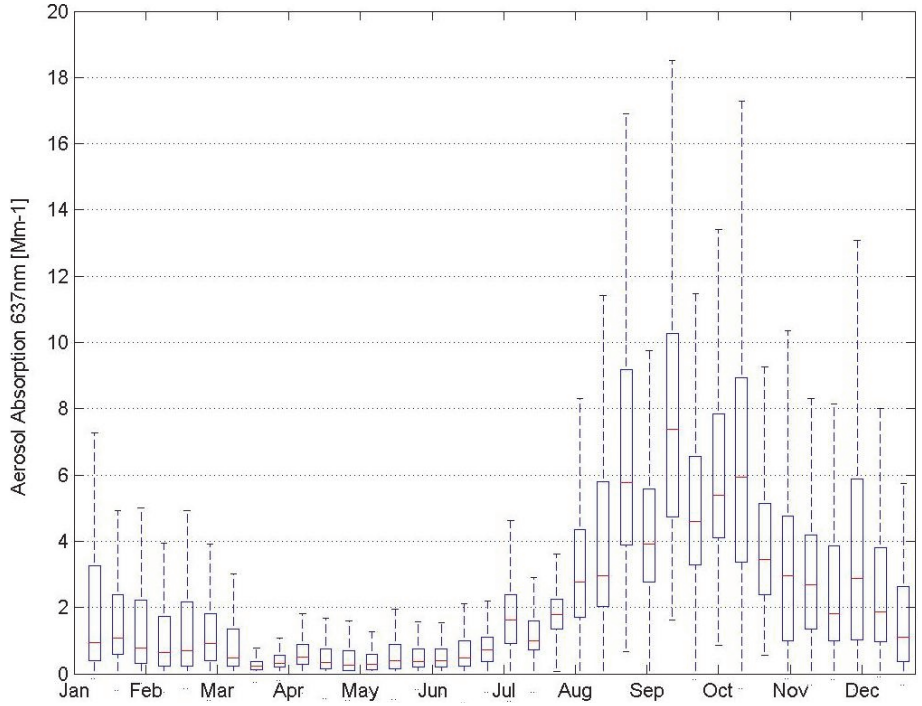

Fig. 11. Box plot considering aerosol particle absorption coefficients at 637 nm between February 2008 and May 2011. Statistics were calculated for each 10 Julian days. The box lines represent the lower quartile, median, and upper quartile values. Whiskers extend within 1.5 times the interquartile range.

ACPD
12, 23333–23401, 2012

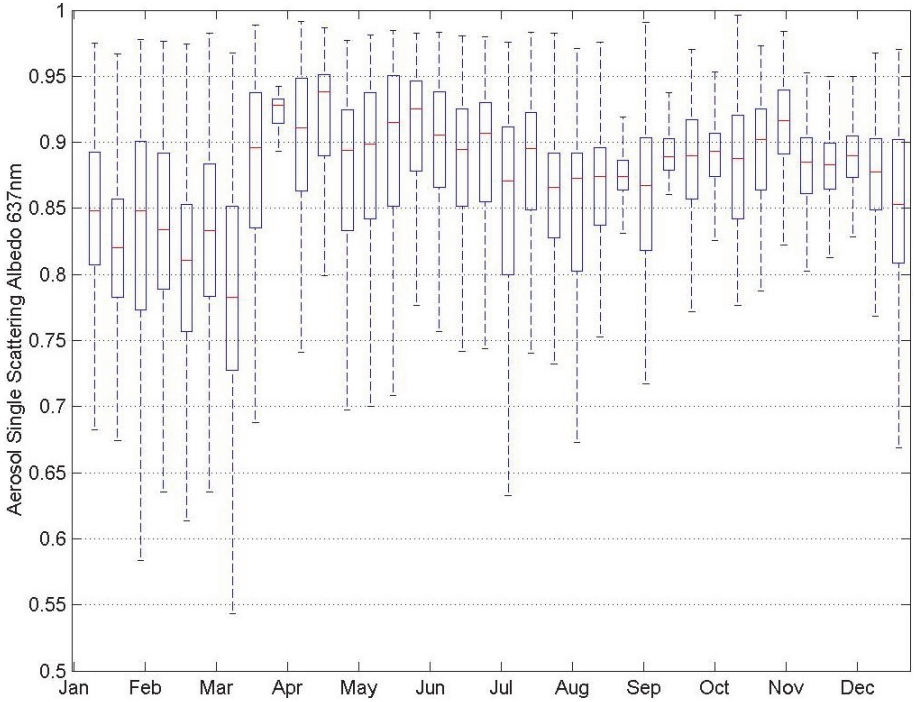

Fig. 12. Box plot considering aerosol single scattering albedo at 637 nm between February 2008 and May 2011. Statistics were calculated for each 10 Julian days. The box lines represent the lower quartile, median, and upper quartile values. Whiskers extend within 1.5 times the interquartile range.

ACPD
12, 23333–23401, 2012

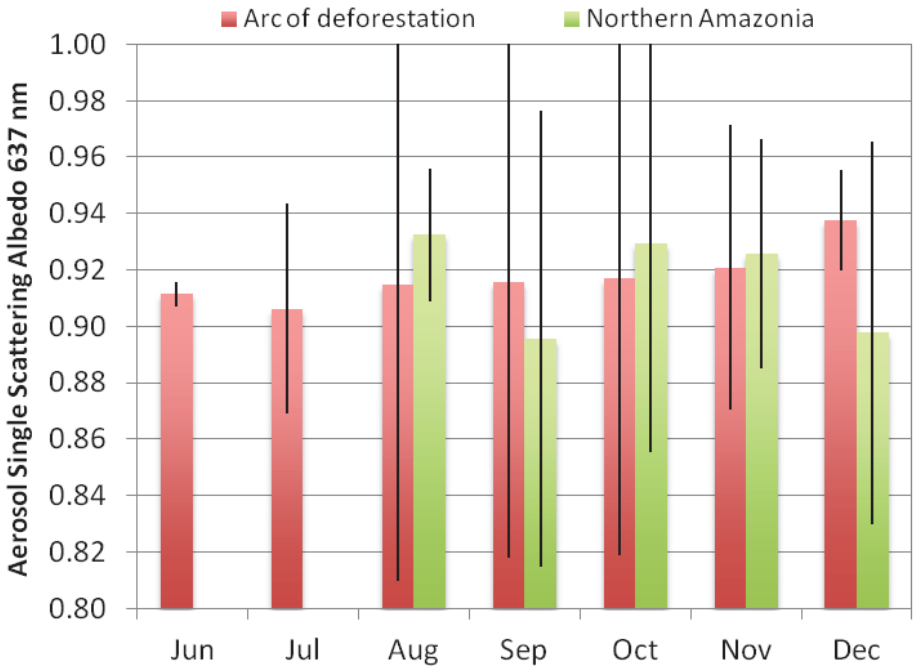

Fig. 13. Monthly averages of AERONET retrieved single scattering albedo between 1993 and 2011 at seven different locations in Amazonia: Ji Paraná, Alta Floresta, Rio Branco (arc of deforestation), Balbina, Belterra, Santarém, Manaus (Northern Amazonia). All data is level 2, with exception to 9 Manaus data points in 2008, which are level 1.5. Particle SSA values observed in the AERONET wavelengths were interpolated to 637 nm. Error bars indicate standard deviations.

ACPD
12, 23333–23401, 2012

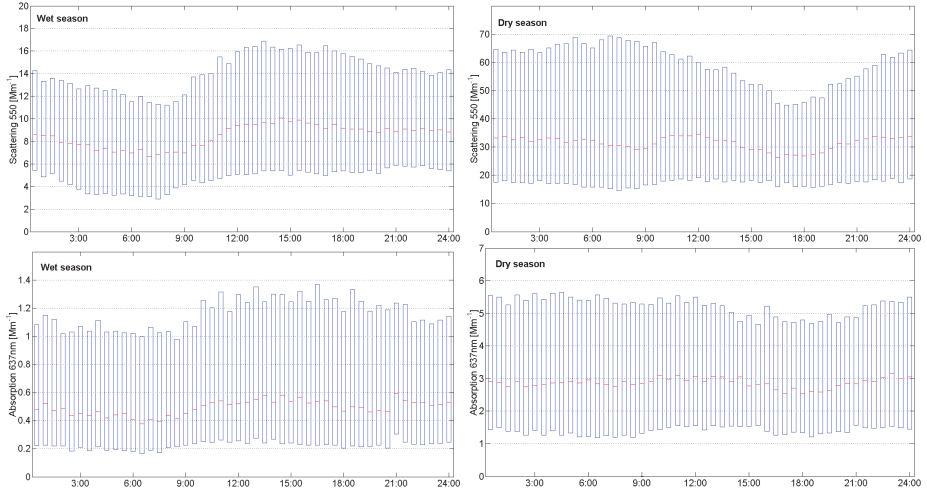

Fig. 14. Local time diel cycle boxplots for **(a)** wet season aerosol particle scattering; **(b)** dry season aerosol particle scattering; **(c)** wet season aerosol particle absorption; **(d)** dry season aerosol particle absorption. The box lines represent the lower quartile, median, and upper quartile values.

ACPD
12, 23333–23401, 2012

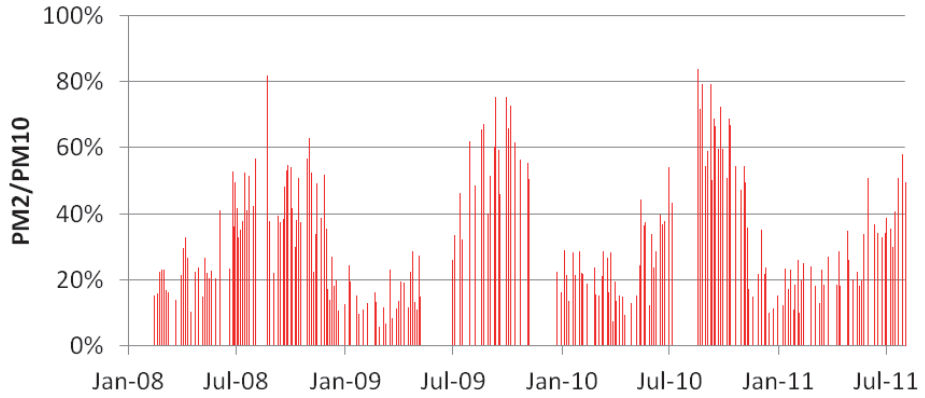

Fig. 15. Contribution of PM_2 to PM_{10} particle mass, observed from gravimetric analysis of 199 stacked filter units samples.

ACPD
12, 23333–23401, 2012

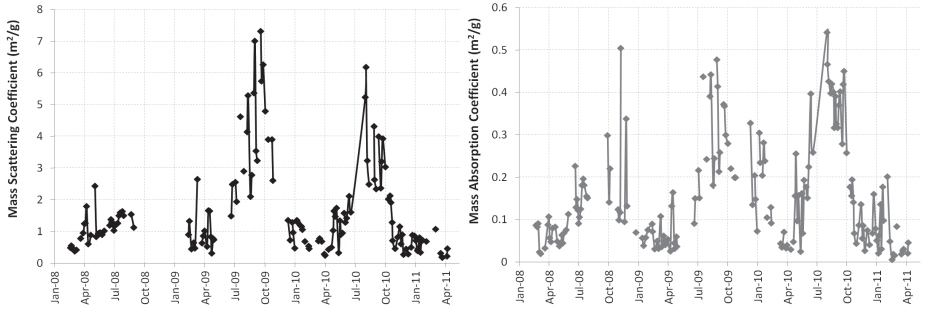

Fig. 16. (a) Particle mass scattering coefficient at 550 nm; **(b)** particle mass absorption coefficient at 637 nm.

ACPD
12, 23333–23401, 2012

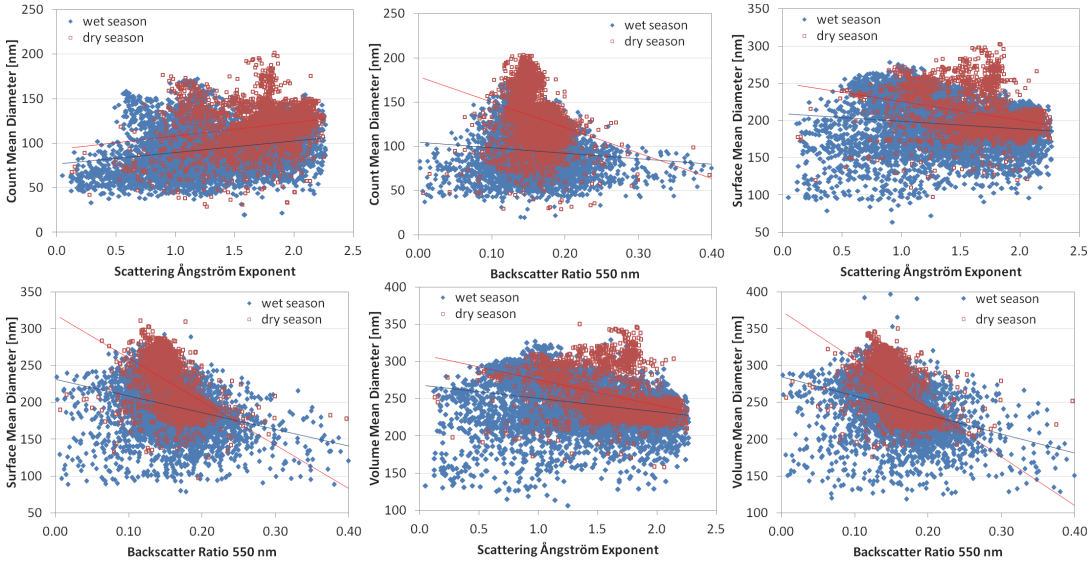

Fig. 17. Relationships between scattering Ångström exponent, backscatter ratio and three parameters calculated from sub micrometer aerosol particle number size distributions (10–500 nm): count mean diameter (CMD), surface area mean diameter (SMD) and volume mean diameter (VMD). The plots comprise measurements taken between November 2009 and July 2010. The lines represent linear fits to the scattered data, to be used as eye guide.

ACPD
12, 23333–23401, 2012

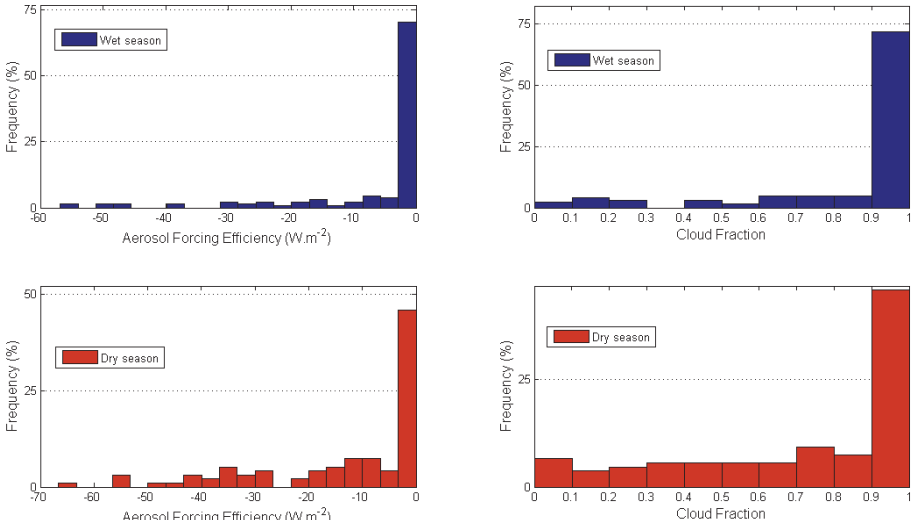

Fig. 18. Frequency histograms for the aerosol forcing efficiency and for the cloud fraction during wet and dry seasons, comprising the period between November 2009 and September 2010.

ACPD
12, 23333–23401, 2012

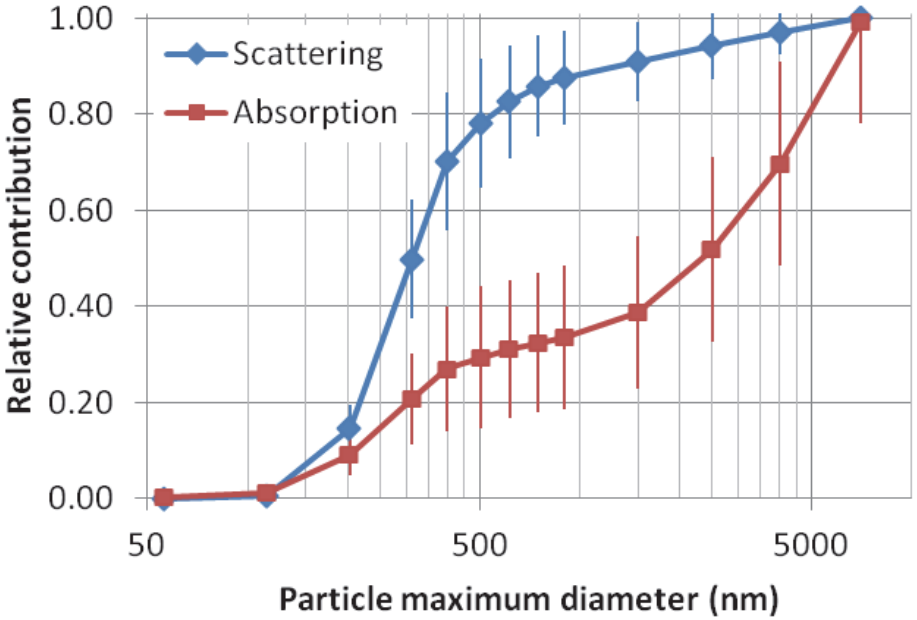

Fig. 19. Cumulative contribution of 13 particle size ranges to scattering (550 nm) and absorption (637 nm) coefficients calculated using a Mie model. Error bars represent standard deviations.

ACPD
12, 23333–23401, 2012

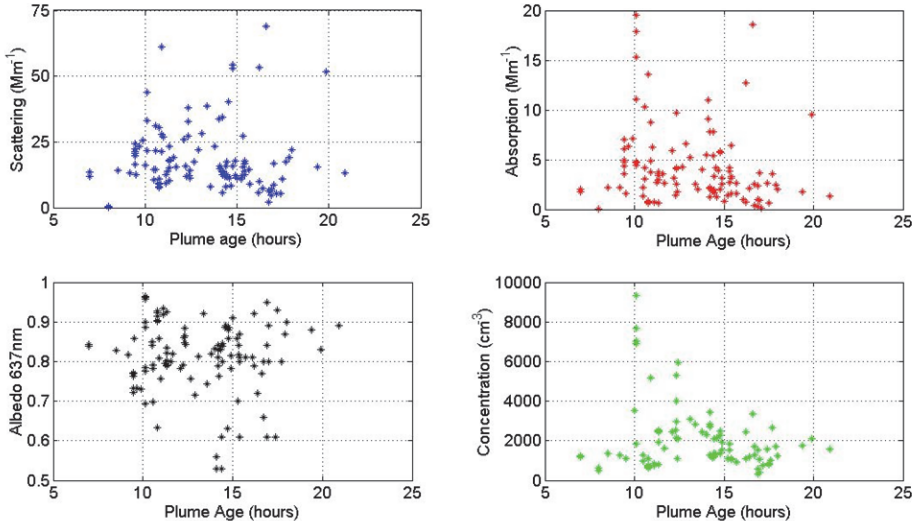

Fig. 20. Aerosol particle properties measured during episodes of Manaus urban plume influence as a function of plume age. **(a)** Scattering coefficient at 550 nm; **(b)** absorption coefficient at 637 nm; **(c)** single scattering albedo at 637 nm; **(d)** aerosol number concentration.

ACPD
12, 23333–23401, 2012

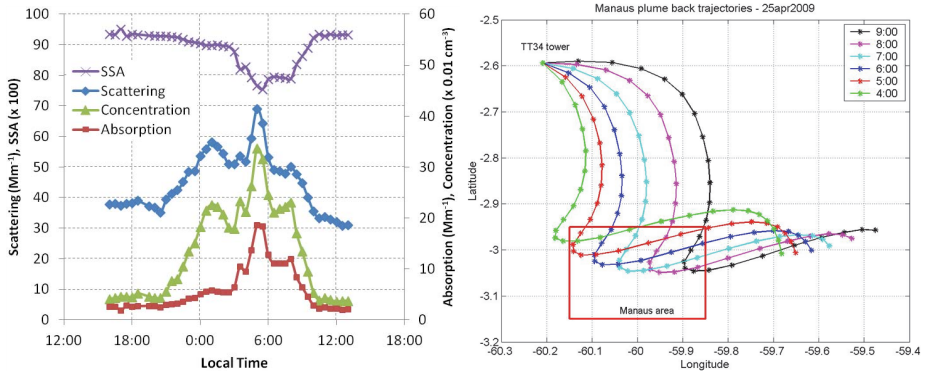

Fig. 21. Example of Manaus urban plume entrance in the research site on 2009 April 25th. **(a)** Evolution of particle single scattering albedo (637 nm), scattering (550 nm), absorption (637 nm) and number concentration; **(b)** HYSPLIT back-trajectories reaching the measurement site at the time specified (local time). Each trajectory point represents one hour less from the start time.

ACPD
12, 23333–23401, 2012